Solar rankine and absorption multi-generation for residential buildings: design, exergy analysis and techno-economic optimization across hemispheric climates

Applied Thermal Engineering 285 (2026) 129307

Contents lists available at ScienceDirect

Applied Thermal Engineering

journal homepage: www.elsevier.com/locate/apthermeng

Research Paper

Solar rankine and absorption multi-generation for residential buildings: design, exergy analysis and techno-economic optimization across hemispheric climates

Ehsanolah Assareh [a,b], Behzad Rismanchi [a], Nima Izadyar [c,d,*], Elmira Jamei [c,d], Alireza Baheri [b], Behdad Barani [b], Saleh Mobayen [e,**], Jagadeesh Kumar Alagarasan [f,***]

[a] Renewable Energy and Energy Efficiency Group, Department of Infrastructure Engineering, Faculty of Engineering and IT, The University of Melbourne, Australia
[b] Strategic Research Institute (SRI), Asia Pacific University of Technology and Innovation (APU), Technology Park Malaysia, Kuala Lumpur, Malaysia
[c] Built Environment and Engineering Program, College of Sport, Health and Engineering (CoSHE), Victoria University, Melbourne, VIC 3011, Australia
[d] Institute for Sustainable Industries and Liveable Cities, Victoria University, Melbourne, VIC 3011, Australia
[e] Graduate School of Intelligent Data Science, National Yunlin University of Science and Technology, Douliou, Yunlin 640301, Taiwan
[f] Department of Chemistry, Faculty of Science, Technology and Architecture (FoSTA), Manipal University Jaipur, Jaipur 303007 Rajasthan, India

ARTICLE INFO

Keywords:
Economic assessment
Energy simulation
Exergy analysis
Multi-objective optimization
Solar thermal systems
Trigeneration

ABSTRACT

Seasonal contrasts between hemispheres pose major challenges to solar energy availability and demand management, yet no previous solar-thermal multi-generation study has systematically evaluated system robustness across mirrored latitudes with opposite seasonal patterns. This study presents a solar thermal multi-generation framework designed to ensure reliable, year-round performance across contrasting hemispheric climates. The proposed system integrates a heliostat field, central receiver, molten-salt thermal storage, a Solar Rankine cycle for power generation, a recuperator for domestic hot water and space heating, and an absorption chiller for cooling. Four representative cities, Sydney and Melbourne (Australia), and Ahvaz and Isfahan (Iran), were selected for their roughly similar latitudes, contrasting climates, and reliable meteorological data, enabling a consistent hemispheric comparison of system adaptability. The methodology combined Building Energy Optimization (BEopt) simulations, thermodynamic modeling in Engineering Equation Solver (EES), and multi-objective optimization using Response Surface Methodology (RSM). Under optimal operation, the system achieved an exergy efficiency of 19.42% producing 1,629.6 MWh of electricity, 10,527.8 MWh of heating, and 1,446.8 MWh of cooling annually in Isfahan. Carbon Dioxide (CO_2) emissions decreased by 332.43 tons per year relative to baseline, and the cost rate was optimized to $169.93/h. The results confirm that the framework maintains stable performance under seasonal reversals, an aspect rarely quantified in solar thermal multi-generation research. The study introduces two key novelties: a hemispheric robustness evaluation framework and a transferable methodology that links building-level demand modeling with thermodynamic simulation and optimization, offering a scalable pathway toward climate-responsive, zero-energy residential systems.

1. Introduction

Recent studies and reports show that, despite improvements in energy efficiency, global building energy consumption and CO_2 emissions remain alarmingly high, representing 32 % of global energy use and 34 % of related emissions [1]. Among different types of buildings, residential settings contribute a significant share of this demand, driven by electricity, heating, and cooling requirements for daily living, making energy efficiency enhancement in the residential sector a worldwide priority [2,3]. Given the global decarbonization goals [4], solar energy stands out for its abundance [5], low environmental impact [6], and

* Corresponding author at: Built Environment and Engineering Program, College of Sport, Health and Engineering (CoSHE), Victoria University, Melbourne, VIC 3011, Australia.
** Corresponding author.
*** Corresponding author.
E-mail addresses: nima.Izadyar@vu.edu.au (N. Izadyar), mobayens@yuntech.edu.tw (S. Mobayen), jaga.jagadeesh1987@gmail.com, jagadeesh.alagarasan@jaipur.manipal.edu (J.K. Alagarasan).

https://doi.org/10.1016/j.applthermaleng.2025.129307
Received 29 August 2025; Received in revised form 22 November 2025; Accepted 28 November 2025
Available online 29 November 2025

Nomenclature

Symbols

A	Surface area of collector or receiver [m^2]
C_P	Specific heat capacity [kJ/kg.K]
E	Pump efficiency [%]
$\dot{E}x$	Exergy rate [kW]
$\dot{E}x_{cooling}$	Exergy associated with cooling [kW]
$\dot{E}x_{heating}$	Exergy associated with heating [kW]
$\dot{E}_{CV}$	Total energy in the control volume [kW]
$\dot{E}_{CV}$	Incident solar exergy rate [kW]
f	Objective function (optimization target)
g	Gravitational acceleration [m/s^2]
h	Specific enthalpy [kJ/kg]
$\dot{m}$	Mass flow rate [kg/s]
n	Project lifetime [years]
N_{hel}	Number of heliostats [-]
P	Pressure [kPa]
P_s	Turbine inlet pressure [kPa]
$\dot{Q}$	Heat transfer rate [kW]
$\dot{Q}_{sun}$	Solar heat rate [kW]
s	Specific entropy [kJ/kg.K]
S_0	Entropy at reference state[kJ/kg.K]
T	Temperature [K]
T_0	Ambient temperature [K]
T_{hot}	Hot tank temperature [K]
T_{cold}	Cold tank temperature [K]
T_{sun}	Solar surface temperature [K]
v	Velocity [m/s]
$\dot{W}$	Work or power [kW]
Z	Component cost function [$]
$\dot{Z}$	Cost rate [$/h]
∅	Operating factor [-]
α	Absorptivity [-]
β	Solar incidence angle [°]
ε	Emissivity [-]
λ	Thermal conductivity [W/m.K]
ρ	Density [kg/m^3]
σ	Stefan–Boltzmann constant (5.67×10^{-8}) [$W/m^2.K^4$]
η	Efficiency
τ	Transmissivity [-]

Abbreviations

BEopt	Building Energy Optimization software
CCD	Central Composite Design
CCHP	Combined Cooling, Heating, and Power
CRF	Capital recovery factor
CSP	Concentrated Solar Power
DNI	Direct Normal Irradiance
DOE	Design of Experiments
EES	Engineering Equation Solver
ERTE	Exergoeconomic Rate of Total Exergy
GA	Genetic Algorithms
LCC	Life Cycle Cost
NPV	Net Present Value
ORC	Organic Rankine Cycle
PSO	Particle Swarm Optimization
PV/T	Photovoltaic/Thermal Collector
RSM	Response Surface Methodology
SM	Solar Multiple
SRC	Solar Rankine Cycle
TRNSYS	Transient System Simulation Tool
ZEB	Zero Energy Building

Subscripts

a	Ambient
abs	Absorber
c	Collector or condenser
cond	Condenser
CV	Control volume
d	Destruction
e	Exit or outlet
eco	Economizer
evap	Evaporator
h	Hot side
hel	Heliostat field
i	Inlet
in	Input
out	Output
opt	Optimum
rec	Receiver
recup	Recuperator
SH	Superheater
tur	Turbine
w	Work

compatibility with existing residential infrastructures [7]. In this context, solar-driven systems, which integrate the simultaneous production of power, heating, and cooling from a single renewable energy source, offer a promising approach [8,9], particularly for residential applications [10,11]. Such systems enhance overall energy efficiency by minimizing energy loss inherent in single-purpose generation [12]. By harnessing locally available solar resources [13], these systems enable seasonally balanced energy optimization and significantly advance the feasibility of achieving Zero-Energy buildings (ZEBs) [14,15]. However, the performance of such systems is strongly influenced by spatial and seasonal variations in solar availability [16], emphasizing the need for adaptable design approaches that respond to climatic and seasonal variability [17].

Researchers have increasingly proposed multi-generation solar systems to meet residential energy demands [9,18]. A study in Famagusta, Cyprus, evaluated a solar-driven trigeneration system, achieving 7.15 kW maximum power output and a minimum electricity cost of 0.1627 $/kWh, demonstrating strong thermodynamic and economic performance [19]. Another investigation optimized solar hybrid Combined Cooling, Heating, and Power (CCHP) systems with energy storage across seven Chinese climates and three building types, reducing optimal device capacities by up to 50 % and improving multi-dimensional benefits [20]. Similarly, a 4E (Energy, Exergy, Economic, and Exergo-environmental) analysis of a solar-powered multi-generation system achieved energy and exergy efficiencies of 12.2 % and 4.3 % with a 3.8-year payback period, confirming its economic viability under varying solar conditions [21]. In another case in St. Petersburg, an integrated system supplying freshwater, power, and heating achieved an environmental sustainability index of 1.13, showing strong environmental and economic performance [22]. Likewise, a solar thermophotovoltaic system designed for a hot, humid region met 35 % of local demand while producing 83 times the required electricity, exporting the surplus to the grid [23]. Across diverse climates, solar-driven multi-generation systems consistently show higher energy and exergy efficiencies, lower operating costs, and improved environmental performance, confirming their adaptability and technical maturity. Further investigations highlight that integrating multiple components enhances both economic feasibility and environmental outcomes; for instance, simulations for

coastal areas reduced electricity consumption by up to 72.3 % in Dubai and 64.6 % in Barcelona, with notable environmental benefits [24]. Collectively, these studies confirm the viability of multi-generation systems in achieving energy savings and sustainability goals [25]. However, to fully harness their potential in residential buildings, particularly across diverse climates, optimal designs must explicitly address variations in solar irradiance, ambient temperature, and occupant-driven demand patterns [26].

To address these climate-dependent variations and improve both cost and efficiency in system design, multi-objective optimization techniques have become essential for balancing the conflicting goals of energy, economic, and environmental performance [12,27,28]. Among these, Response Surface Methodology (RSM) has gained prominence for its clarity, flexibility, and computational efficiency in modeling complex energy systems with interacting variables [29–31]. Unlike purely heuristic methods such as Genetic Algorithms (GAs) or Particle Swarm Optimization (PSO), RSM's regression-based surrogates enable sensitivity analysis and efficient Pareto trade-offs with far fewer simulations [32], as demonstrated in recent solar-assisted studies [33,34]. Recent review papers highlight the growing application of hybrid multi-objective optimization frameworks that integrate RSM with heuristic and simulation-based approaches to balance thermodynamic, economic, and environmental objectives in renewable energy systems [35,36]. Recent multi-objective optimization studies on solar-based multi-generation and CCHP systems have demonstrated thermodynamic and economic performance improvements [9,37]. For example, a 4E optimization of a solar thermal CCHP system using RSM achieved 55.3 % exergy and 25.6 % thermal efficiency while reducing unit cost and environmental impact by 4.8 % and 3.3 %, confirming the capability of RSM to balance thermodynamic and economic objectives [38].

While RSM provides transparent and computationally efficient optimization, its polynomial structure limits accuracy in highly nonlinear or dynamically varying conditions, such as those driven by climate and occupant behavior [34]. To overcome these limitations, RSM can be coupled with Building Energy Optimization (BEopt) and Engineering Equation Solver (EES) thermodynamic modeling, particularly for residential settings [15,39]. This integration aligns building-level energy demand with component-level generation performance, supporting climate-responsive, cost-effective, and robust system design across diverse climates. In recent studies, combining BEopt and EES with RSM improved model representativeness by linking simulated demand with real system responses, achieving energy efficiency gains up to 25 % and cost reductions of 10–15 %, depending on climate and configuration [25,40]. However, integrated simulation and optimization of building and system performance remain largely overlooked in existing studies [41,42]. These challenges are compounded by the variability of solar irradiance and temperature across climates, directly influencing system output and efficiency [43,44]. Evaluating performance across hemispheric contexts, with reversed seasonal cycles and distinct solar distributions, is therefore essential for assessing robustness and scalability, yet such analyses are scarce [45–47]. To date, no comprehensive study has systematically compared solar-based multi-generation systems across both hemispheres under consistent optimization and building typologies, despite the importance of hemispheric evaluation for ensuring transferable, climate-responsive designs.

To address this research gap, the present study develops and optimizes a solar-based multi-generation energy system specifically designed for residential buildings and rigorously evaluates its performance in contrasting hemispheric climates. Accordingly, this study pursues three specific objectives designed to translate the identified research gap into a structured, measurable framework for analysis. The objectives of this research are as follows: (1) to design and optimize a multi-generation solar energy system for a typical 16-unit residential building, (2) to evaluate its performance across four strategically selected cities, Sydney and Melbourne in Australia (Southern Hemisphere), and Ahvaz and Isfahan in Iran (Northern Hemisphere), which share similar latitudes yet exhibit reversed seasons and distinct climates, and (3) to assess system effectiveness through critical metrics including exergy efficiency, operational cost rates, and CO_2 emission reduction potential. The novelty of this work lies in (i) establishing a unified hemispheric framework for the first cross-latitude comparison of solar-driven multi-generation systems under consistent boundary and optimization conditions, (ii) coupling BEopt-based building energy simulations with detailed thermodynamic modeling through RSM to bridge building-scale demand and system-scale performance, and (iii) introducing an integrated Exergy–Economic–Environmental (3E) assessment framework that transforms conventional optimization into a transferable design methodology for resilient and climate-adaptive residential energy systems. Under the optimized configuration, the proposed system achieved up to 19.42 % exergy efficiency and an annual CO_2 reduction of 332 tons, confirming the framework's technical robustness and real engineering viability. By achieving these objectives, this study extends current thermal engineering knowledge by providing a robust and transferable framework for designing solar-driven multi-generation systems that are efficient, cost-effective, and climate-adaptive. Section 2 describes the methodology, Section 3 details the system design and simulation process, Section 4 presents and discusses the results, Section 5 outlines limitations and future work, and Section 6 concludes the study.

2. Methodology

The overall process, illustrated in Fig. 1, provides a structured framework designed to be reliable, scalable, and adaptable across diverse seasonal and climatic conditions. The methodology for developing and evaluating the proposed multi-generation solar energy system comprises five sequential stages: 2.1 Energy Demand Simulation, 2.2 System Modeling, 2.3 Multi-Objective Optimization, 2.4 Performance Analysis, and 2.5 Economic Analysis.

2.1. Energy demand simulation

The first stage involved simulating the building's annual energy demand using BEopt software to accurately estimate the electricity, heating, and cooling requirements of a representative 16-unit residential complex. The process began with defining the geometrical layout and structural envelope characteristics of the selected building, ensuring compliance with standard Australian construction specifications. Hourly meteorological data were then sourced from Meteonorm [48] for four representative cities, Melbourne and Sydney in Australia, and Ahvaz and Isfahan in Iran, to capture contrasting climatic and hemispheric conditions. BEopt's simulation outputs provided detailed energy profiles for each location, quantifying seasonal variations in total and end-use energy demand. These data formed the foundation for designing the system's thermal and electrical generation capacities and for evaluating overall performance under diverse climatic scenarios.

2.2. System modeling

In the second stage, a solar-driven multi-generation energy system was developed based on BEopt-derived demand profiles. The system was designed to cogenerate electricity, heating, and cooling. Annual thermodynamic system performance was modeled using Engineering Equation Solver (EES), which enabled the solution of coupled energy and exergy balance equations across the system's components. The modeling procedure included defining the system configuration, specifying boundary conditions, and validating results against established Rankine-cycle benchmarks in the literature [49].

To ensure reproducibility, all simulation parameters, boundary conditions, and component-specific equations were explicitly defined in Appendix A. Input data such as ambient temperature, solar irradiation, and working-fluid properties were obtained from Meteonorm and the

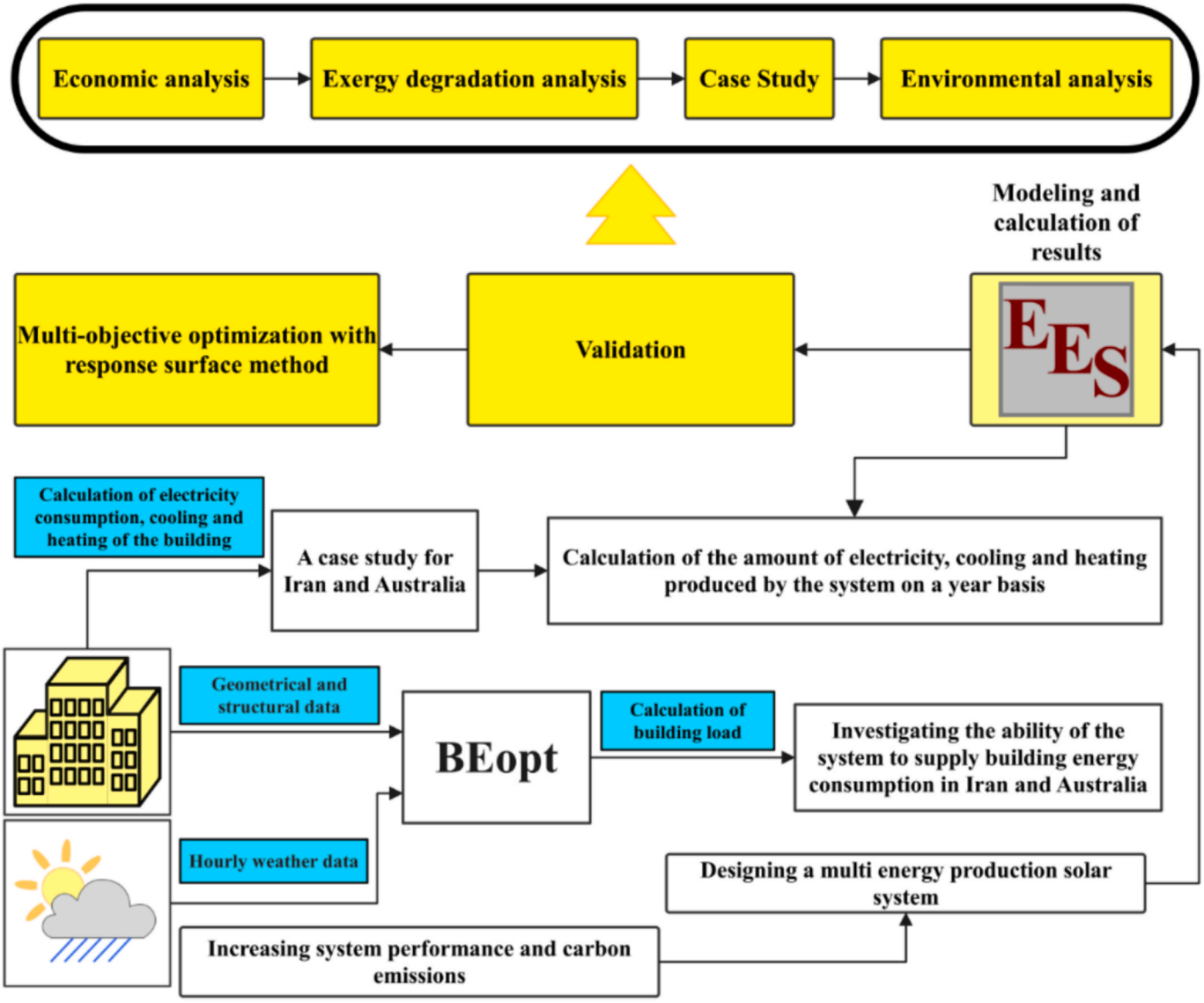

Fig. 1. Whole image of the proposed methodology.

REFPROP thermophysical database integrated into EES. Each major component, turbine, pump, economizer, evaporator, condenser, superheater, and absorber, was modeled under steady-state assumptions, neglecting minor heat losses. The corresponding control volumes and state numbering presented in the system schematic enable complete replication of the energy and exergy balance formulations summarized in Appendix Table A1.

2.3. Multi-objective optimization

The third stage focused on optimizing system performance using RSM implemented in Minitab 21 [50]. This procedure aims to identify Pareto-optimal configurations that simultaneously maximize exergy efficiency and minimize the overall cost rate. Six design variables, including turbine and pump efficiencies, were selected for their significant influence on thermodynamic and economic performance. A Central Composite Design (CCD) comprising 90 simulation runs was employed to generate the experimental matrix and construct quadratic polynomial regression models representing system behavior over the design space. The optimization was performed using a desirability function-based algorithm, which converts each objective into a dimensionless scale ranging from 0 (undesirable) to 1 (fully desirable) and maximizes the overall desirability index. This approach is widely adopted in RSM-based multi-objective studies for its computational efficiency, smooth convergence, and ability to balance conflicting objectives without requiring gradient-based solvers [51]. Model adequacy was verified using Analysis of Variance (ANOVA) tests, residual diagnostics, and R^2 validation to confirm statistical reliability and predictive accuracy before determining optimal configurations. The resulting response surfaces, regression models, and optimization equations are summarized in Appendix Table A4, with further validation details provided in Section 3.4.

2.4. Performance analysis

Following optimization, the system's technical, economic, and environmental performance was comprehensively evaluated under each climatic condition. Utilizing EES software and Sankey diagram visualization tools, exergy degradation and energy distribution were analyzed to identify major sources of loss and potential improvement. The performance analysis also integrated an economic assessment to examine operational cost variations across the four climatic zones. Furthermore, the system's environmental performance was evaluated by quantifying annual reductions in CO_2 emissions, demonstrating its contribution to

climate change mitigation and alignment with global sustainability targets.

2.5. Economic analysis

The final stage addressed the economic feasibility of the proposed multi-generation system. The cost rate ($\dot{Z}$) was calculated for each component and for the total system, incorporating both capital investment and maintenance costs. These costs were annualized using the Capital Recovery Factor (CRF) as defined in Appendix A (Table A1). A project lifetime of 20 years and a discount rate of 10 % were assumed, consistent with industry practice for solar-thermal installations. The electricity tariff was set at 0.18 $/kWh, representing the average residential rate used for comparative analysis. Detailed cost correlations for all components, including the receiver, heliostat field, turbine, pump, condenser, evaporator, and thermal storage tanks, are summarized in Appendix A (Tables A1 and A4). These parameters ensure full reproducibility of the economic evaluation and maintain consistency with the thermodynamic model.

Fig. 1 illustrates the workflow of the methodological approach adopted in this study.

3. System design and simulation

This section provides a detailed description of each stage outlined in the methodology, beginning with the case study context and input data preparation. The simulation starts by defining the building configuration and climatic conditions, which serve as the basis for calculating residential energy demands. These demand profiles guide the conceptual design of a solar-driven multi-generation system, which is then thermodynamically modeled and validated. Subsequent sections describe the optimization strategy used to improve energy performance and cost-effectiveness, followed by a comprehensive analysis of technical, environmental, and economic outcomes.

3.1. Case study and energy demand simulation

This study designs and optimizes a solar-based multi-generation energy system for a residential apartment in four cities: Melbourne and Sydney in Australia (Southern Hemisphere) and Ahvaz and Isfahan in Iran (Northern Hemisphere). These cities were strategically selected due to their roughly similar latitudes but contrasting hemispheric positions, allowing a controlled assessment of hemispheric seasonal inversion and its impact on energy performance. Each city represents a distinct climate: Melbourne (blue) has an oceanic climate with cool winters and

Fig. 2. Geographic locations and coordinates of the studied cities, spanning from the southeast (Melbourne, −37.81°S) to the northeast (Isfahan, 32.65°N).

mild summers; Sydney (green) is humid subtropical with warm summers and mild winters; Ahvaz (red) has a desert climate with extremely hot summers and mild winters; and Isfahan (yellow) experiences a semi-arid climate characterized by hot, dry summers and chilly winters.

The selection of these four cities followed specific criteria to ensure methodological consistency and meaningful comparison across hemispheres. The primary criterion was latitude similarity (ranging between 32° and 38° north/south), which allows direct evaluation of seasonal inversion effects on solar resource utilization and building thermal demand. The second criterion was climatic diversity, guided by the Köppen–Geiger classification [52], ensuring representation of four dominant climate types, oceanic (Cfb), humid subtropical (Cfa), desert (BWh), and semi-arid (BSh), to capture a wide range of thermal and solar profiles. The third criterion was data reliability: all four locations have validated hourly meteorological datasets available through Meteonorm [48], compatible with both BEopt and EES for consistent simulation inputs. Lastly, these cities were chosen for their representativeness of major residential regions with differing building energy regulations and solar potential, enhancing the generalizability and practical relevance of the system design outcomes. Fig. 2 illustrates the geographic distribution and coordinates of the study cities, spanning from the southeast (Melbourne, −37.81°S) to the northeast (Isfahan, 32.65°N).

The selected case study is a 16-unit apartment, representative of typical medium-density housing frequently found in urban areas. This scale was chosen to accurately reflect realistic energy consumption patterns and improve the practical relevance of the results for urban energy policies, building code formulation, and retrofit strategies. Given the growing global prevalence of multi-family dwellings, studying this building type ensures broad applicability and ease of replication. The building features a pier-and-beam foundation and is oriented towards the north to maximize natural daylighting and passive solar gains, thereby improving its overall energy efficiency. Table 1 shows the main specifications of the building model.

To ensure realistic simulations, hourly weather files containing ambient temperature, wind speed, solar irradiation, and relative humidity, critical parameters in assessing system efficiency, were sourced using Meteonorm [48]. Meteonorm was selected due to its reliable global coverage, ability to generate high-resolution hourly datasets, and compatibility with BEopt and EES software. These features ensure consistent and accurate climate modeling across all four selected cities, forming a reliable foundation for the subsequent simulation and performance evaluation phases of the study.

Fig. 3 presents the monthly climatic profiles of the four studied cities: Melbourne, Sydney, Ahvaz, and Isfahan, showing variations in ambient temperature, solar irradiation, wind speed, and relative humidity. These parameters define the boundary conditions for energy-demand simulation and thermodynamic performance modeling. The profiles highlight the strong hemispheric and seasonal contrasts that test the adaptability of the proposed multi-generation solar system. Ahvaz and Isfahan, representing hot and arid climates, record the highest ambient temperatures and solar irradiation from May to August, with peaks of approximately 39.2 °C and 324 W/m^2, respectively, indicating high summer cooling loads but excellent solar-thermal harvesting potential. In contrast, Melbourne and Sydney exhibit moderate summer temperatures (20–23 °C) and lower solar irradiation during June–August, reflecting the reversed seasonal pattern of the Southern Hemisphere and necessitating flexible thermal-storage operation to maintain year-round stability. Wind speeds are consistently higher in Melbourne (4.7–6.0 m/s) and moderate in Sydney (3.0–3.6 m/s), enhancing convective cooling and supporting opportunities for hybrid ventilation integration. By comparison, lower wind intensities in Ahvaz and Isfahan (below 3.0 m/s) limit passive cooling potential. Relative humidity further distinguishes the climatic conditions: Melbourne and Sydney sustain higher humidity (above 70 % in cooler months), increasing latent loads, whereas Ahvaz and Isfahan experience very dry summers (below 25 %), which reduces evaporative cooling efficiency. Together, these climatic characteristics govern the heating and cooling demand profiles, influence collector sizing and control strategies, and ultimately determine the exergy efficiency of the system, emphasizing the necessity of a design that can adapt across divergent hemispheric and climatic contexts.

Table 1
Key specifications of the residential building model.

Specifications	Unit	Value
Number of Floors	–	4
Floor Area per Level	m^2	360
Total Building Area	m^2	1440

Fig. 4 presents the step-by-step workflow used to analyze the building's energy performance, beginning with city selection and climate data collection and progressing through building design, material selection, and simulation using BEopt software. The flowchart captures the full process, from defining the 16-unit, four-story residential building and incorporating localized weather data to optimizing material choices and calculating electricity, heating, and cooling loads. This structured approach helps identify key variables for improving energy efficiency and supports data-driven decisions in building design.

The energy demands of the 16-unit residential building, including electricity, space heating, and cooling, were modeled using BEopt software, which is specifically developed for optimizing residential building performance. Unlike general-purpose tools such as EnergyPlus and TRNSYS, which require extensive customization and calibration, BEopt offers a streamlined, user-friendly interface tailored to residential contexts. It integrates building geometry, occupancy schedules, construction materials, and hourly weather data to perform high-fidelity simulations while leveraging the EnergyPlus engine under the hood. BEopt's parametric analysis and built-in optimization framework enable efficient comparison of design alternatives and selection of cost-effective, energy-efficient solutions across various climates. Because this study adopts a steady-state modeling approach, BEopt provides accurate load estimations without the computational complexity of dynamic simulations. Its outputs, hourly profiles of electricity, heating, and cooling demands, form the foundation for sizing and evaluating the proposed solar-driven multi-generation system, ensuring both technical precision and practical relevance across diverse hemispheric conditions.

To enhance energy performance across varying climates, a range of building materials and construction assemblies were evaluated using BEopt's parametric simulation framework. This process involved 90 simulation iterations over approximately 15 h to identify optimal combinations tailored to the thermal and economic requirements of each city. The iterative modeling accounted for insulation types, wall and roof assemblies, glazing, and shading configurations. The results reflect the sensitivity of energy performance to local climatic factors and construction material properties. For example, Sydney's optimal configuration included R-20 open-cell spray foam and high-performance glazing to address humidity and moderate temperatures, while Isfahan required R-30C fiberglass roof insulation and light brick façades to manage its hot, dry conditions. Table 2 summarizes the best-performing material selections for Ahvaz, Sydney, Isfahan, and Melbourne, balancing thermal efficiency with cost-effectiveness for each specific climate.

To further assess energy performance across the four climates, the monthly energy consumption for electricity, heating, and cooling was analyzed based on the BEopt simulation outputs. As shown in Fig. 5, electricity consumption varies significantly between cities due to seasonal shifts and climate-specific needs. In the colder months (June to August), Melbourne and Sydney show a rise in electricity use in the selected building, with Melbourne reaching over 21,000 kWh in July. In contrast, Ahvaz and Isfahan exhibit lower electricity demand during this period but experience sharp increases in the warmer months. Notably, Ahvaz's electricity consumption peaks at 18,066 kWh in August, about

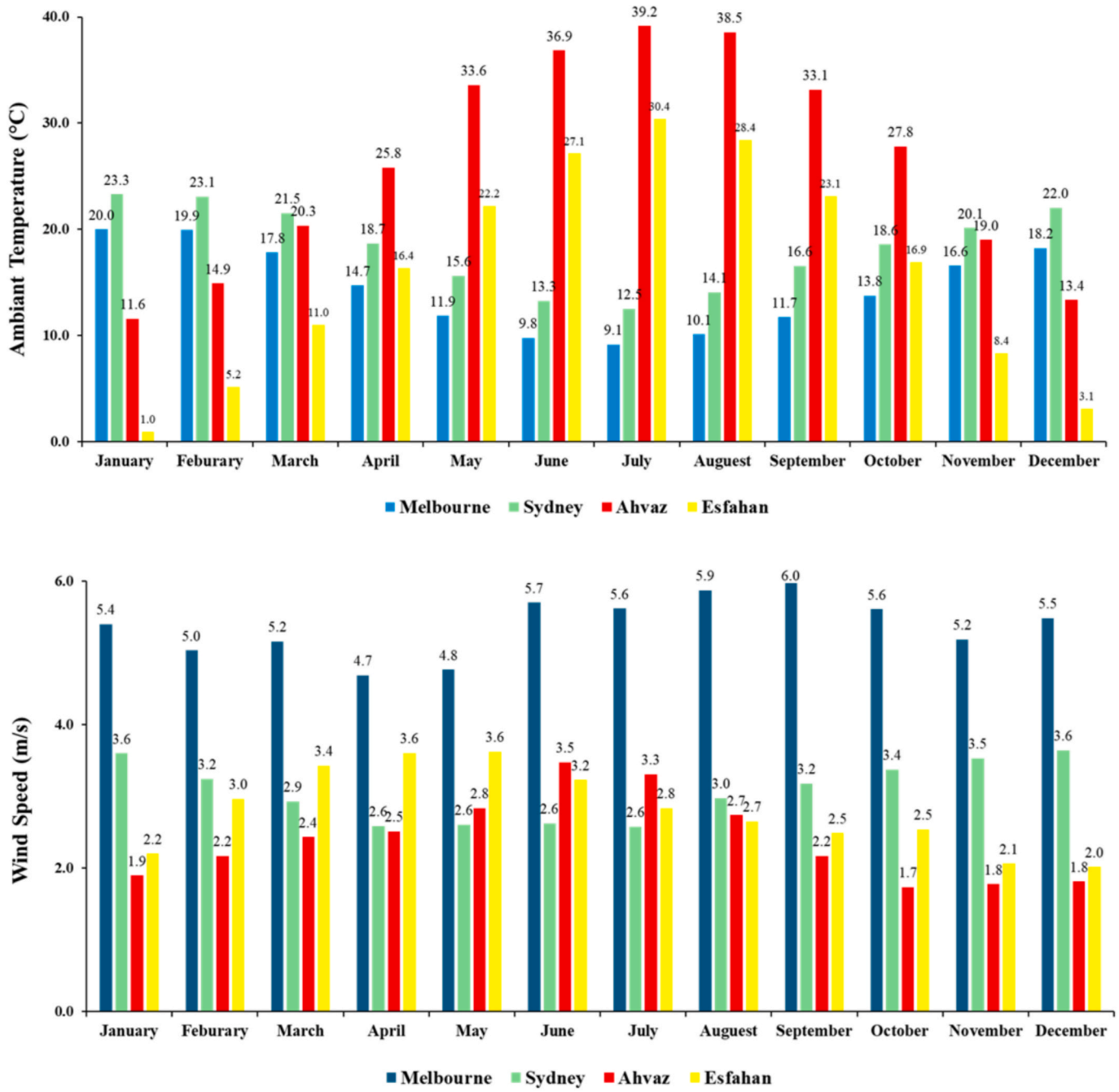

Fig. 3. Climatic profiles of the studied cities.

1.7 times higher than Melbourne's July peak. Isfahan also shows an elevated summer demand, though more balanced, with its highest electricity use recorded in August at 12,046 kWh.

Heating and cooling demand further highlight the climatic contrasts. The case study building's heating consumption in Melbourne reaches 3,587 kWh in July, nearly nine times greater than that of the same building in Ahvaz, reflecting the cold winter in Melbourne and the mild winter in Ahvaz. Meanwhile, Ahvaz's cooling load in July surges to over 69,000 kWh, which is more than five times higher than Melbourne's peak cooling in February (13,652 kWh), and nearly double that of Sydney in the same month. Isfahan presents a dual demand profile, requiring 6,609 kWh of heating in January and 56,063 kWh of cooling in July, indicating the need for year-round adaptability. These differences highlight the importance of an efficient and flexible multi-generation system, capable of accommodating diverse energy loads, seasonal inversion, and varying solar availability across climates.

The economic and environmental implications of the energy demand scenarios were evaluated through cost and emission metrics. Table 3 presents a comparative analysis of annualized energy costs, life cycle costs, and CO_2 emissions for each city. Ahvaz exhibits the highest annualized and life cycle energy costs (2,044.48 $/yr and $76,133.75, respectively), along with the highest CO_2 emissions (0.005 tCO_2/yr), due to its extreme climate and higher cooling demand. In contrast, Sydney shows the lowest annualized energy costs (1,307.76 $/yr) and CO_2 emissions (0.003 tCO_2/yr), reflecting milder weather conditions and more balanced seasonal energy requirements. While Isfahan's energy costs fall between those of Ahvaz and Melbourne, it achieves the lowest energy savings source (0.5 %), highlighting the challenges of

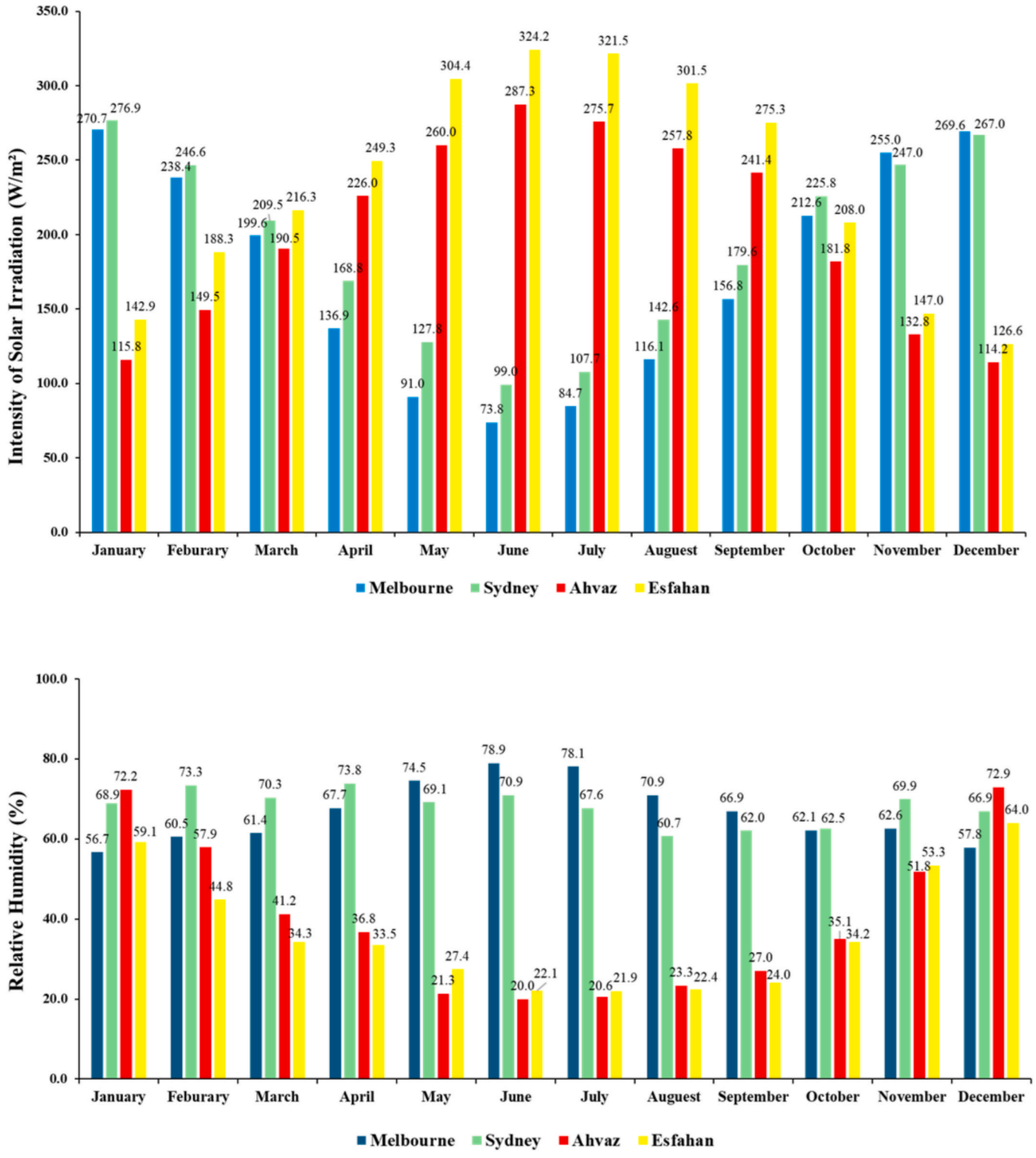

Fig. 3. (*continued*).

optimizing energy performance in semi-arid climates. Melbourne demonstrates moderate energy costs and emissions, with a relatively high source energy savings rate (1.73 %), indicating effective material and design choices under temperate conditions. These findings illustrate how climatic context strongly influences both operational costs and environmental performance, emphasizing the importance of climate-adaptive system optimization for effective multi-generation energy planning.

3.2. Solar-driven multi-generation system modeling

In this study, a solar-based multi-generation energy system is developed to simultaneously supply electricity, heating, and cooling in residential buildings in different climates. The system integrates concentrated solar power with a modified Solar Rankine Cycle (SRC), supported by thermal storage units and an absorption-based cooling subsystem. This configuration is designed to reduce energy losses,

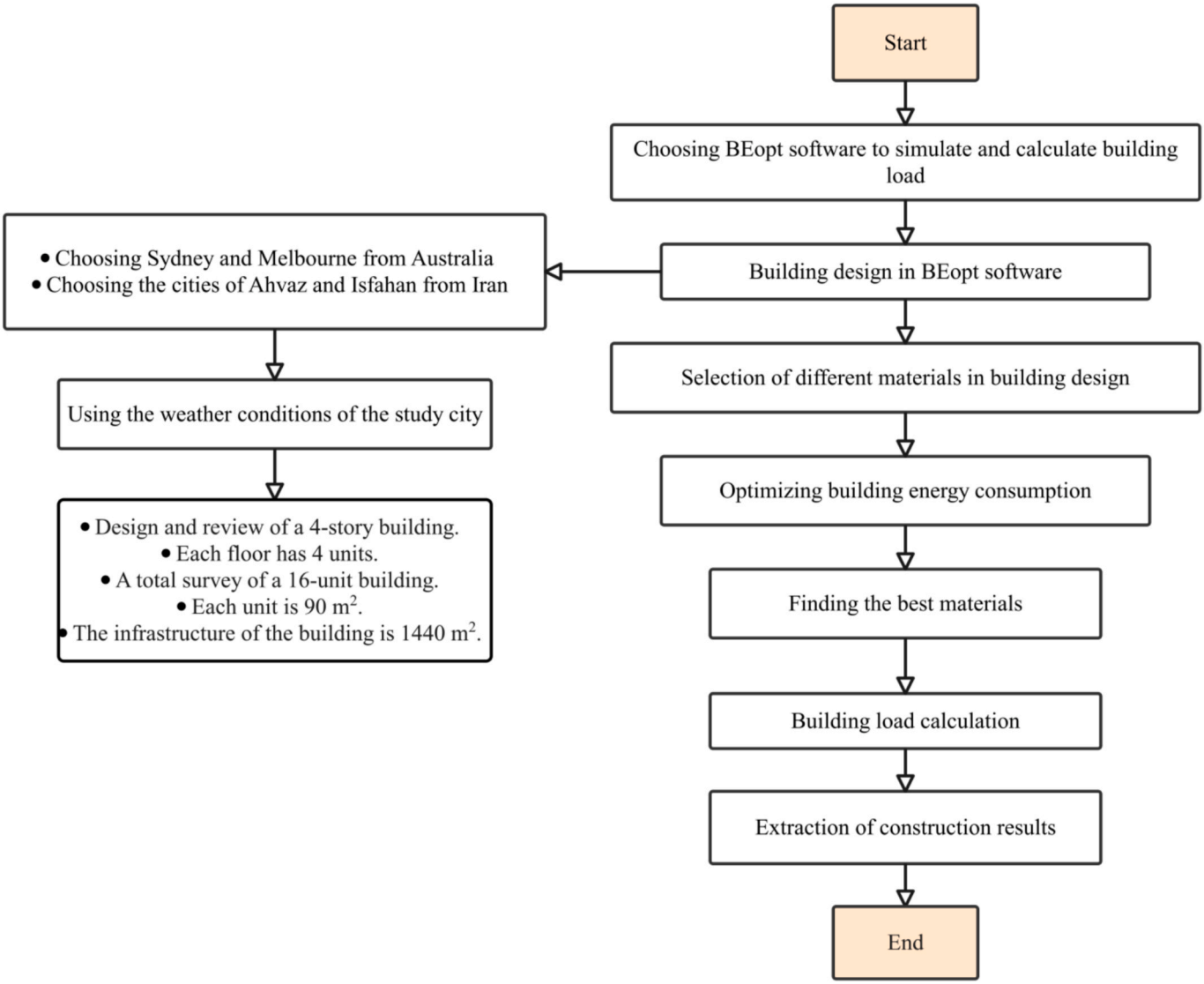

Fig. 4. Flowchart of building energy consumption modeling.

enhance overall efficiency, and maintain continuous operation under varying seasonal fluctuations. By leveraging concentrated solar thermal energy, the system supports sustainable energy generation tailored to diverse climatic conditions while aligning with energy self-sufficiency and carbon reduction targets.

The proposed configuration comprises three core subsystems: (1) a solar thermal collection and storage unit, (2) an electricity and heating generation loop, and (3) an absorption refrigeration unit. As shown in Fig. 6, solar energy is collected by a heliostat field and directed toward a central receiver, where the working fluid (e.g., molten salt) is heated. The heated fluid is stored in a hot storage tank before being pressurized by a pump and passed through an economizer, evaporator, and superheater. It then enters a turbine to produce electricity. The exhaust fluid from the turbine is recovered via a recuperator, supplying thermal energy (approximately 80 °C) for building heating and domestic hot water. Additionally, part of the working fluid is directed into an absorption cooling cycle, consisting of components such as an evaporator, condenser, absorber, and generator, to provide cooling. A cold storage tank ensures operational continuity during low solar periods. The system also includes a separator to optimize thermodynamic efficiency by splitting vapor and liquid phases, with flow regulated by a series of valves and pumps.

To define the solar field, 250 heliostats were modeled, each with a reflective area of 50 m2, arranged in a radial-staggered north-field configuration to minimize cosine and shading losses. This corresponds to a total reflective area of about 12,500 m2 and an effective optical aperture of 10,600 m2 at the design Direct Normal Irradiance (DNI) of 850 W/m2. The central receiver was rated as a nominal thermal capacity of 9.5 MWh, yielding a Solar Multiple (SM) of 1.5 relative to the SRC's design thermal input. The molten-salt storage tanks, hot (773 K) and cold (573 K), were sized to provide roughly 6 h of full-load operation, consistent with medium-scale tower plant practice. These design parameters follow typical Concentrated Solar Power (CSP) tower configurations reported in recent guidelines and reviews, specifically a Solar Multiple (SM) in the range 1.5–2.5. 6–10 h of two-tank molten-salt storage and radial-staggered heliostat fields, consistent with the National Renewable Energy Laboratory (NREL)'s Annual Technology Baseline (ATB) 2024 CSP power-tower baseline [53] and the International Energy Agency (IEA) CSP technology briefs [54].

Overall, the integrated solar-driven tri-generation system is engineered to reliably and efficiently meet year-round energy demands of residential buildings across different climates. Uniform flow distribution in the system's piping was assumed to ensure consistent thermal exchange across components and to simplify hydraulic modeling. A constant convective heat transfer coefficient was assumed for the receiver and piping surfaces to simplify the thermal analysis of solar energy

Table 2
Optimized construction material configurations for each selected city.

Optimal choice	Ahvaz	Sydney	Isfahan	Melbourne
Wood Stud	R-13 Fiberglass Batt, 2 × 4, 16 in on center	R-20 Open Cell Spray Foam, 2 × 4, 16 in on center	R-15 Fiberglass Batt, 2 × 4, 16 in on center	R-13 Fiberglass Batt, 2 × 4, 16 in on center
Wall Sheathing	R-5 × PS	R-15 × PS	OSB	OSB, R-6 Polyiso
Exterior Finish	Vinyl, Light	Fiber-Cement, Medium/Dark	Brick, Light	Fiber-Cement, Medium/Dark
Interzonal Walls	R-13 Open-Cell Spray Foam, 2 × 4, 16 in on center	R-23 Closed-Cell Spray Foam, 2 × 4, 16 in on center	R-13 Fiberglass Batt, 2 × 4, 16 in on center. R-6 Polyiso	R-23 Closed-Cell Spray Foam, 2 × 4, 16 in on center
Finished Roof	R-47.5 SIPs	R-27.5 SIPs	R-30C Fiberglass Batt, 2 × 10	R-30C Fiberglass Batt, 2 × 10
Roof Material	Asphalt Shingles, Light	Asphalt Shingles, Light	Metal, Light	Galvanized Steel
Pier & Beam	Ceiling R-13 Fiberglass Batt	Ceiling R-19 Fiberglass Batt	Ceiling R-38 Open-Cell Spray Foam	Ceiling R-19 Open-Cell Spray Foam
Carpet	40 % Carpet	60 % Carpet	60 % Carpet	
Floor Mass	Wood Surface	2 in, Gypsum Concrete	2 in, Gypsum Concrete	2 in, Gypsum Concrete
Exterior Wall Mass	1.2 in, Drywall	2 × 5.8 in, Drywall	1.2 in, Drywall	Drywall/PCM Mat
Partition Wall Mass	2 × 5.8 in, Drywall	Drywall/PCM Mat	1.2 in, Drywall	2 × 5.8 in, Drywall
Ceiling Mass	1.2 in, Drywall	2 × 5.8 in, Drywall	2 × 5.8 in, Drywall	PCM Drywall
Window Areas	F15 B15 L15 R15	F18 B15 L15 R15	F15 B15 L15 R15	F18 B18 L18 R18
Windows	Back Windows=High-SHGC	Low-E, Double, Non-metal, Air, L-Gain	Clear, Double, Metal, Air	Low-E, Double, Non-metal, Air, L-Gain
Interior Shading	Summer = 0.7, winter = 0.7	Summer = 0.6, winter = 0.7	Summer = 0.7, winter = 0.7	Summer = 0.7, winter = 0.95
Door Area	20 ft^2	30 ft^2	20 ft^2	40 ft^2
Doors	Steel	Fiberglass	Wood	Fiberglass
Eaves	2 ft	2 ft	1 ft	3 ft
Overhangs	2 ft, First Story, Left Windows	2 ft, First Story, Front Windows	2 ft, First Story, All Windows	2 ft, First Story, All Windows
Lighting	60 % CLF	100 % Incandescent	80 % LED	40 % LED
Double wood stud	R-33 Fiberglass Batt, Gr-1, 2 × 4 Centered, 24 in on center	R-45 Fiberglass Batt, Gr-1, 2 × 4 Staggered, 24 in on center	R-33 Fiberglass Batt, Gr-1, 2 × 4 Centered, 24 in on center	R-39 Fiberglass Batt, Gr-1, 2 × 4 Centered, 24 in on center
Steel stud	R-21 Fiberglass Batt, 2 × 4, 24 in on center	R-25 Fiberglass Batt, 2 × 8, 24 in on center	R-11 Fiberglass Batt, 2 × 4, 24 in on center	R-13 Fiberglass Batt, 2 × 4, 24 in on center

capture and transport.

3.3. Thermodynamic simulation and validation

To simulate the performance of the proposed solar-driven multi-generation system, the EES software was employed due to its robustness in modeling complex thermodynamic systems involving multiple energy flows. EES provides a flexible, equation-based platform that allows users to define and solve custom sets of algebraic and differential equations, ideal for multi-generation systems that integrate electricity production, space heating, and cooling. Unlike many commercial tools that rely on fixed system configurations, EES enables detailed component-level customization, accurately capturing the dynamic energy exchanges between subsystems such as the solar thermal input, storage tanks, turbine system, recuperator, and absorption cooling cycle. Its built-in thermodynamic property database supports a wide range of fluids and materials relevant to solar-thermal applications, ensuring high-fidelity system modeling. The thermodynamic analysis was conducted under steady-state conditions to simplify the modeling process and minimize the effects of transient fluctuations. Side heat losses from insulated components were assumed negligible, and energy transfer within the system was considered quasi-steady-state, allowing the use of simplified energy and exergy equations while maintaining accuracy across seasonal variations.

The EES-based model was developed by defining energy and exergy balance equations for each component in the system. The heliostat field, receiver, thermal storage tanks, economizer, evaporator, superheater, turbine, recuperator, and absorption chiller were all mathematically represented within EES. Using this framework, a comprehensive input–output dataset was generated, detailing the system's thermal, electrical, and cooling outputs under varying climatic inputs. Each simulation scenario reflected city-specific weather conditions and energy demand profiles generated in BEopt. Through EES's parametric analysis capabilities, the effects of key design parameters, such as working fluid temperatures, turbine efficiency, and recuperator effectiveness, were examined for all climate zones. This parametric analysis served as a foundation for the subsequent optimization stage.

The simulation results were exported into a structured dataset containing both input variables and corresponding objective function outputs (e.g., electricity generated, cost rate, and exergy efficiency). This dataset was then used in the multi-objective optimization process to identify Pareto-optimal configurations. By applying these refined parameters, the system demonstrated the capacity to simultaneously produce electricity, space heating, and cooling at a high efficiency, even under diverse and reversed seasonal conditions. EES's ability to flexibly simulate steady-state thermodynamic models, evaluate system sensitivity, and accurately capture integrated energy flows confirms its suitability for evaluating real-world solar-based multi-generation systems. This ensures the system's scalability and adaptability in both hemispheric contexts while supporting annual energy reliability and sustainability goals.

To validate the thermodynamic accuracy of the proposed solar-driven multi-generation system, a comparative Rankine cycle simulation was conducted using EES and benchmarked against the reference study [49]. Validation involved a parameter-by-parameter comparison of critical variables governing the Rankine cycle's thermodynamic integrity. Specifically, the heat source temperature and turbine inlet pressure were verified to ensure that the modeled heat addition and expansion processes replicated the boundary conditions of the reference system. The mass flow rate was included to account for its influence on working fluid circulation, energy balance, and power generation. Turbine power and overall system efficiency were compared to confirm accurate mechanical-to-electrical conversion and consistent energy integration. As summarized in Table 4, the simulation results demonstrate strong agreement with the benchmark, with deviations of only 0.0185 % for turbine power and 0.428 % for system efficiency. These minimal differences validate the robustness of the developed model and confirm its reliability for representing the integrated thermodynamic and solar-thermal systems.

While only the Rankine cycle subsystem is compared with benchmark data, this is justified given its central role in the system's energy conversion chain and aligns with standard validation practices in multi-

	January	Feburary	March	April	May	June	July	Auguest	September	October	November	December
Melbourne	21619.14	18888.78	15948.10	13033.50	11300.66	10518.38	10787.67	12078.26	14548.78	17507.82	20736.94	21869.44
Sydney	22320.64	19501.69	16465.59	13456.41	11667.35	10859.68	11137.71	12470.18	15020.87	18075.92	21409.82	20339.07
Ahvaz	26788.75	23405.44	19761.66	16150.14	14002.95	13033.54	13367.29	14966.46	18027.75	21694.34	25695.58	17689.54
Isfahan	22317.65	19499.08	16463.38	13454.61	11665.79	10858.22	11136.22	12468.51	15018.86	18073.50	21406.95	14737.09

	January	Feburary	March	April	May	June	July	Auguest	September	October	November	December
Melbourne	486.81	852.55	1528.31	8239.35	23220.25	33677.66	25340.51	23736.03	21305.49	9065.21	3647.29	26379.55
Sydney	0.00	0.00	0.00	700.80	6981.86	15846.75	34408.41	23299.58	8791.44	15.01	76.30	0.00
Isfahan	93657.21	59168.46	26444.49	8029.87	194.00	0.00	0.00	0.00	0.00	465.25	28827.69	60399.40
Ahvaz	2216.66	276.42	0.00	0.00	0.00	0.00	0.00	0.00	0.00	0.00	0.00	438.21

	January	Feburary	March	April	May	June	July	Auguest	September	October	November	December
Melbourne	15682.79	22073.39	12460.90	0.00	0.00	0.00	0.00	0.00	0.00	0.00	0.00	0.00
Sydney	37369.91	34434.58	20015.98	6240.94	0.00	0.00	4.15	67.29	0.00	0.00	7517.00	9998.78
Ahvaz	8227.34	12224.64	32136.40	56054.24	94106.92	115348.18	131335.76	121273.15	107326.49	77199.74	35668.00	3009.57
Isfahan	0.00	0.00	0.00	5104.59	19837.33	50633.39	69315.43	62941.82	30133.81	8237.02	0.00	0.00

Fig. 5. Monthly electricity, heating, and cooling usage of the case study across selected cities.

Table 3
Economic and environmental performance metrics by city.

Performance metric	Unit	Sydney	Ahvaz	Isfahan	Melbourne
Annualized energy costs	$/yr	1307.760	2044.480	1642.720	1473.800
Net present value of energy costs	$	1431.080	2237.840	1443.300	1619.450
Life cycle energy costs	$	60710.500	76133.750	67676.300	64008.570
Source energy savings	%/yr	1.020	2.690	0.500	1.730
CO_2 emissions	tCO_2/yr	0.00310	0.00500	0.00410	0.00370
CO_2 savings	%/yr	1.02	2.71	0.44	1.59

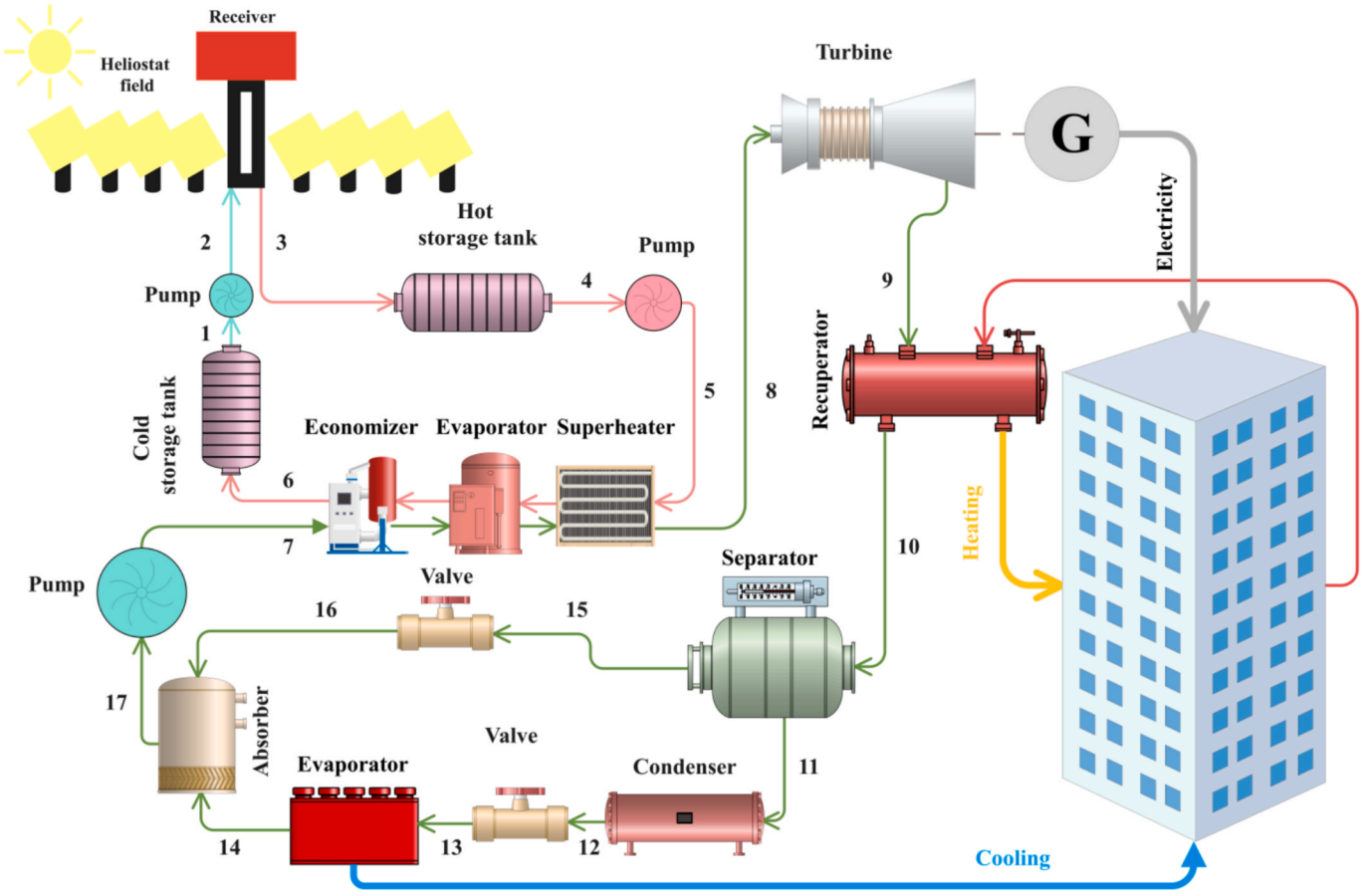

Fig. 6. Schematic of the proposed solar-driven multi-generation system.

Table 4
Validation of the thermodynamic model against the reference study [49].

Parameter	Unit	Current study	Referenced study	Error (%)
Source temperature	K	573	573	–
Mass flow rate (Input)	kg/s	0.86	0.836	2.870
Turbine inlet pressure (P_8)	kPa	398.8	398.8	–
Turbine power	kW	541.2	541.3	0.0185
Net system power	kW	519.3	516.6	0.523
System energy efficiency	%	14.09	14.03	0.428

energy modeling studies [55].

3.4. Multi-objective optimization and performance evaluation

To improve the overall performance and viability of the proposed solar-driven multi-generation system, multi-objective optimization was performed using RSM implemented in Minitab 21 [50]. RSM is a powerful statistical technique that is particularly well-suited for optimizing complex systems influenced by multiple interacting variables [56,57]. In this study, it was selected for its ability to generate accurate predictive models, identify Pareto-optimal solutions, and balance competing objectives such as energy efficiency and cost-effectiveness. Minitab's integrated Design of Experiments (DOE) and regression tools provided an efficient platform for constructing response surfaces and rapidly evaluating various design configurations across the different climatic conditions of the four studied cities.

In this research, RSM was used to explore how key design variables interact and influence system outcomes, with the dual objective of maximizing exergy efficiency and minimizing operational cost rate. Table 5 summarizes the selected variables and their respective ranges, including heliostat number (200–400), turbine inlet pressure (20–40 kPa), turbine and pump efficiencies (70 %–95 %), and hot and cold tank temperatures (750–900 K and 500–650 K, respectively), all of which are critical to system performance. By systematically varying these parameters, RSM developed predictive models revealing system sensitivity to each factor and identifying optimal design configurations. This structured approach supports informed trade-off decisions between performance and cost under different climatic conditions.

Table 5
Design variables and ranges used in RSM optimization.

Parameter	Unit	Lower value	Upper value
Heliostat number	–	200	400
Turbine inlet pressure (P_8)	kPa	20	40
Cold tank temperature	K	500	650
Hot tank temperature	K	750	900
Pump efficiency	%	70	95
Turbine efficiency	%	70	95

The optimization targeted two key objectives: maximizing Exergoeconomic Rate of Total Exergy (ERTE) to minimize system energy loss and minimizing operational cost rate to enhance economic feasibility. Six key decision variables were selected based on their thermodynamic and economic impact: heliostat number, turbine inlet pressure (P8), cold and hot thermal storage temperatures, and the efficiencies of both the pump and turbine. A total of 90 simulation runs were conducted in Minitab, with RSM applied to build predictive models and determine the optimal settings.

These 90 simulations were structured using Minitab's DOE framework, which systematically explored combinations of the selected parameters. This iterative approach enabled sensitivity analysis of how each factor influences ERTE and cost rate, facilitating the identification of Pareto-optimal configurations. The wide parameter coverage demonstrated the robustness and practical value of the RSM-based framework for refining multi-variable renewable energy systems.

To illustrate the optimization process, Table 6 presents a representative sample of ten runs showing trade-offs between ERTE and cost rate. As observed, configurations achieving higher ERTE generally incur higher costs, while others achieve more balanced performance. This emphasizes the importance of multi-objective optimization for identifying efficient, economically viable system configurations. The complete dataset of 90 runs is provided in Appendix B (Table B1) to support reproducibility and transparency.

The final optimal configuration, obtained using composite desirability scoring, is summarized in Table 7. It includes 210 heliostats, a turbine inlet pressure of 40 kPa, cold and hot tank temperatures of 660 K and 980 K, respectively, and pump and turbine efficiencies of 0.94 and 0.863. These parameters delivered strong performance outcomes, as summarized in Table 8, achieving an ERTE of 19.42 % and an operational cost rate of $169.93/hour. The composite desirability index of 0.928 confirms close alignment with the ideal multi-objective targets, where values near 1 indicate simultaneous satisfaction of efficiency and cost objectives. These results demonstrate the effectiveness of RSM in tuning complex, multi-variable energy systems for practical renewable applications.

To contextualize the optimization outcomes, Table 9 summarizes the observed range of performance metrics across all simulations. The results highlight the system's sensitivity to design parameter variations, showing substantial potential for performance gains through optimization.

To further enhance system optimization and enable sensitivity analyses, regression equations were also developed for the two objective functions: cost rate and ERTE, to enable rapid prediction of system behavior under varying input conditions. These equations serve as practical tools for real-time decision-making, design adjustment, and extended sensitivity analyses. For simplicity, each variable was assigned an identifier (Table 10), facilitating compact regression formulation and interpretation.

Eqs. (1) and (2) represent the regression models for cost rate and ERTE, respectively, based on the selected design variables.

To complement the optimization, a detailed performance evaluation was conducted. Exergy degradation was analyzed using Sankey diagrams to visualize energy flows and losses within the system, providing insight into inefficiencies and guiding future design improvements. The system's environmental impact was assessed through annual CO_2 emissions reductions, confirming its contribution to decarbonization efforts. An economic assessment compared operating costs across climates, illustrating how financial viability varies with local conditions. This integrated evaluation confirms that the proposed system is technically optimized, environmentally sustainable, and economically feasible across diverse hemispheric settings.

Fig. 7 illustrates the structured workflow of the RSM applied in this study. The process begins with the selection of independent variables and definitions of the test area, followed by the path of steepest descent to approach the optimal region. The CCD is then used to plan the DOE, introducing decision variables and their ranges. Results from the simulations are used to fit a quadratic regression model, validated for accuracy, reliability, and predictive capability. Once validated, the model is used to determine the optimal values of the objective functions. This methodology enables systematic exploration of complex variable interactions through iterative simulation and model validation, leading to optimal configurations that maximize ERTE and minimize cost rate. Its application demonstrates RSM's effectiveness as a robust and replicable framework for advancing the design, evaluation, and control of high-performance renewable energy systems under diverse climatic conditions.

4. Results and discussion

This section presents the outcomes of energy simulations and the optimization aimed at improving the system's overall performance. By using RSM, key design variables were optimized to achieve greater efficiency and cost-effectiveness. The following subsections discuss the results in detail, examining both technical and economic performance under varying climatic conditions across the selected cities. The findings highlight how different design parameters impact the system's ability to meet residential energy demands while reducing operational costs and CO_2 emissions.

$$\begin{aligned} Costrate = {} & 68.58 + 0.8364A + 0.3381B - 0.2614C - 0.00368D - 1.0E - 1.43F - 0.000030A^*A - 0.00671B^*B + 0.000213C^*C + \\ & 0.000052D^*D - 0.03E^*E + 0.41F^*F + 0.000921A^*B - 0.000244A^*C - 0.000157A^*D + 0.03332A^*E + 0.00033A^*F + \\ & 0.000003B^*C - 0.000080B^*D + 0.2475B^*E - 0.0196B^*F + 0.000013C^*D + 0.00079C^*E + 0.00373C^*F - 0.00462D^* \\ & F - 0.00065D^*F - 0.81E^*F \end{aligned} \quad (1)$$

$$\begin{aligned} ERTE(\%) = {} & -9.98 - 0.01004A + 0.1507B + 0.00043C + 0.04047D + 1.11E + 2.09F - 0.000028A^*A - 0.001528B^*B - 0.000001C^*C - 0.000019D^* \\ & D + 1.64E^*E - 1.05F^*F + 0.000039A^*B - 0.000001A^*C + 0.000040A^*D + 0.001988A^*E + 0.000168A^*F + 0.000002B^*C - 0.000107B^* \\ & D + 0.11494P8(kPa)^*E + 0.00190B^*F + 0.000001C^*D + 0.000542C^*E + 0.000593C^*F - 0.005692D^*E - 0.000786D^*F - 0.017E^*F \end{aligned} \quad (2)$$

Table 6
Selected optimization runs highlighting parameter effects on ERTE and cost rate.

Run	Heliostat number	P8 (kPa)	Cold tank temp (K)	Hot tank temp (K)	Pump Eff.	Turbine Eff.	ERTE (%)	Cost rate ($/h)
2	400	40	500	900	0.95	0.70	21.25	291.6
4	200	20	500	900	0.70	0.95	16.82	159.6
7	200	40	650	900	0.95	0.70	18.87	159.2
15	200	20	500	750	0.7	0.7	15.15	152
21	200	40	650	750	0.95	0.95	17.80	151.4
33	400	40	650	900	0.95	0.95	21.28	276.5
41	300	30	575	890	0.825	0.825	19.24	217.9
47	200	20	650	750	0.70	0.95	15.17	144.2
67	400	40	500	750	0.95	0.95	18.96	288.5
90	200	40	500	900	0.95	0.95	18.89	166.5

Table 7
Optimal values of decision variables obtained from RSM.

Solution	Unit	Value
Heliostat number	–	210
Turbine inlet pressure (P_8)	kPa	40
Cold tank temperature	K	660
Hot tank temperature	K	980
Pump efficiency	%	0.94
Turbine efficiency	%	0.863426

Table 8
Optimized system performance and composite desirability.

Solution	Unit	Value
ERTE	%	19.42
Cost Rate	$/h	169.93
Composite Desirability	–	0.93

Table 9
Observed range of optimization outcomes.

Metric	Unit	Target	Lower	Upper
Cost Rate	$/h	Minimize	144.20	291.60
ERTE	%	Maximize	15.15	21.28

4.1. Multi-objective optimization

The results of multi-objective optimization demonstrate how the main design parameters affect the system's exergy efficiency (ERTE). As shown in Fig. 8, the interaction effects of turbine inlet pressure, pump efficiency, hot tank temperature, and heliostat number were examined using response surface plots. A consistent trend was observed across all combinations: increasing each parameter leads to a notable improvement in exergy efficiency. Particularly, higher turbine inlet pressures (P_8) and pump efficiencies shift system performance from below 17 % ERTE to over 19.5 %, indicating a substantial gain in thermodynamic quality. Similarly, raising the hot tank temperature from 750 K to 1000 K, particularly when combined with improved pump performance or elevated turbine pressure, increases ERTE beyond 20 %. Moreover, increasing the number of heliostats from 200 to 400 enhances system efficiency, especially at turbine pressures above 35 kPa. These patterns confirm that the design parameters are not only individually important but also synergistically improve exergy efficiency when optimized together. The target exergy efficiency of 19.42 % was achieved through this optimization, underscoring the carefully calibrated system inputs in improving overall performance.

Fig. 9 shows the combined influence of key design parameters on the system's cost rate, with the primary goal of minimizing operating costs. The contour plots show that five major variables: heliostat number, turbine inlet pressure (P_8), pump efficiency, and hot and cold tank temperatures, have significant effects on cost performance. Increasing pump efficiency and reducing the hot tank temperature markedly lowers the cost rate, with values falling below $212/h, particularly when pump efficiency exceeds 90 %. Similarly, lower hot tank temperatures paired with moderate turbine inlet pressures (around 25–30 kPa) consistently reduce operating costs. Conversely, increasing the number of heliostats and cold tank temperature substantially raises costs, with the rate exceeding $280/h when heliostat counts surpass 350 and cold tank temperatures exceed 620 K. The lowest cost rate achieved through this optimization was $169.93/h, confirming that cost efficiency results from the balanced interaction of multiple parameters rather than the dominance of a single factor. This analysis demonstrates that optimal economic performance depends on the coordinated tuning of interdependent design variables that collectively determine the overall cost behavior of the multi-generation system.

4.2. Economic evaluation of system components

To better understand the cost structure of the proposed solar-driven multi-generation system, a detailed component-level economic analysis was conducted. Fig. 10 presents the distribution of operational costs, divided into two major subsystems: the solar unit and the SRC unit. The total system cost rate was estimated at $160.55/h, with the solar unit being the dominant contributor at $135.06/h, representing more than 80 % of the total cost. Within this unit, the heliostat field alone accounts for $86.69/h, followed by the receiver at $48.33/h, making them the two most cost-intensive components. The SRC unit, with a cost rate of $25.49/h, is primarily influenced by the turbine ($12.61/h) and the two evaporators ($6.05/h and $7.57/h), while other components, such as pumps and tanks, contribute minimally (mostly under $1/h). This breakdown clearly indicates that cost optimization efforts should focus on the solar subsystem, particularly the heliostat field and receiver, to achieve the most significant reductions in overall system cost.

4.3. Exergy analysis

Fig. 11 illustrates the exergy distribution and losses within the proposed multi-generation system under optimized operating conditions. The process begins with a solar exergy input of 27,895 kWh, of which a significant portion (15,190 kWh) is lost in the heliostat field, leaving 12,705 kWh delivered to the receiver. The receiver then loses 8,842

Table 10
Assigned identifiers for optimization parameters used in regression equations.

Decision parameters	Unit	Identifier
Heliostat number	–	A
Turbine inlet pressure (P_8)	kPa	B
Cold tank temperature	K	C
Hot tank temperature (^{0}K)	K	D
Pump efficiency (%)	%	E
Turbine efficiency (%)	%	F

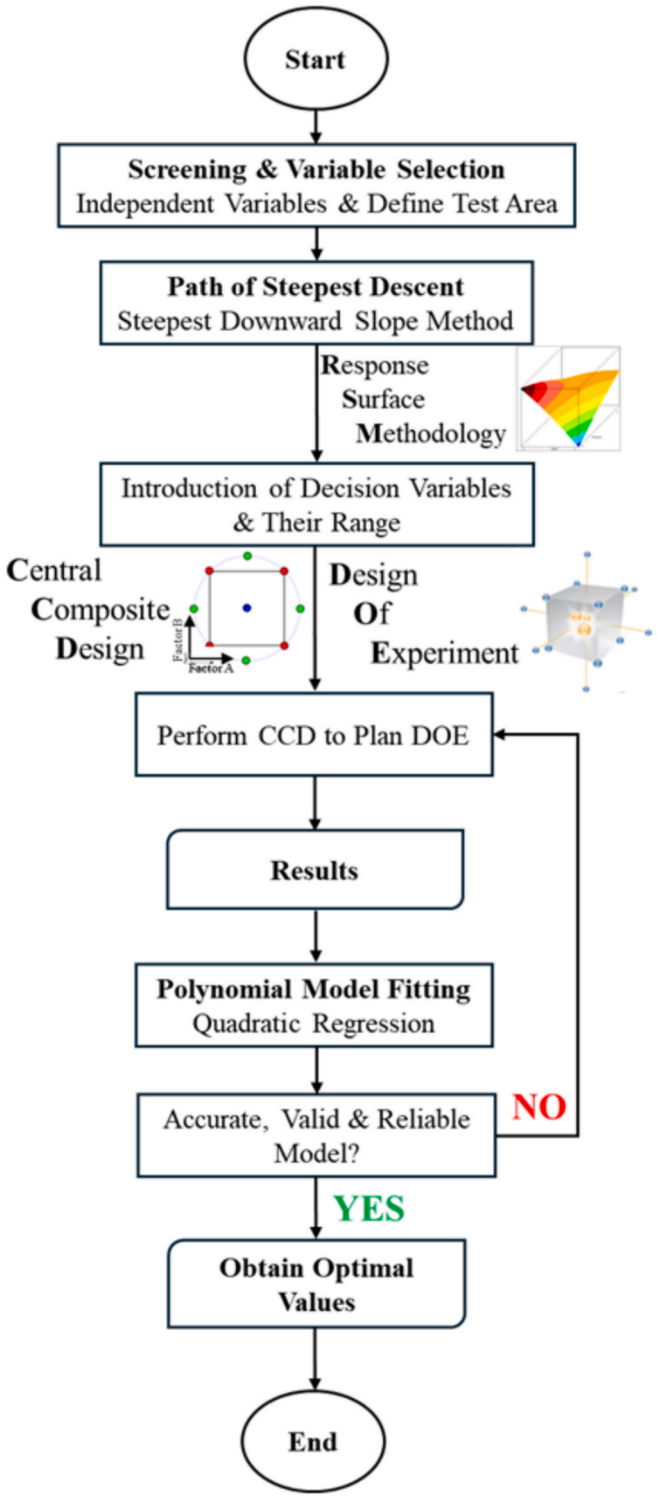

Fig. 7. The systematic application of the response surface methodology.

kWh, passing 3,992 kWh to the superheater. From this point, the system generates 808 kWh of electricity through the turbine, although 318 kWh is lost due to conversion inefficiencies. The recuperator utilizes 2,459 kWh to deliver 1,413 kWh of useful heating, while the evaporator converts 614 kWh into 454 kWh of cooling output. The largest exergy destruction occurs in the heliostat field, receiver, and turbine, which together account for the majority of the system's total exergy loss of 25,220 kWh. This analysis highlights the critical need for targeted design improvements in solar collection and heat transfer components to enhance the system's overall thermodynamic performance.

4.4. Energy and environmental performance across selected cities

To evaluate the adaptability and efficiency of the proposed system under diverse climatic conditions, the analysis was conducted across four cities: Isfahan, Ahvaz, Sydney, and Melbourne. This assessment examines how geographic location, local climate, and seasonal variations influence power generation, heating, and cooling performance. Fig. 12 displays the monthly electricity generation across the four cities, clearly reflecting the impact of seasonal solar availability and hemispheric inversion. Isfahan consistently produces the highest electricity output between May and August, peaking at 219,600 kWh in July, followed by Ahvaz, which reaches 210,312 kWh in June, driven by strong solar irradiance during the summer of the Northern Hemisphere. In contrast, Melbourne and Sydney reach their electricity generation peaks during December and January, with Melbourne attaining 180,768 kWh, consistent with the Southern Hemisphere summer. During their respective winters (June–August for Melbourne and Sydney), electricity output declines by up to 85 % compared with summer months. This pronounced seasonal inversion underscores the importance of location-specific system optimization to ensure consistent, stable year-round performance and efficient solar utilization across hemispheres.

Fig. 13 illustrates the monthly heating generation from the recuperator in Melbourne, Sydney, Ahvaz, and Isfahan, showing substantial seasonal variation linked to climatic patterns. Isfahan and Ahvaz, both located in the Northern Hemisphere, experienced a steady increase in heating output from May through August, with Isfahan peaking at 1,419,120 kWh in July and Ahvaz reaching 1,140,800 kWh. These values reflect enhanced thermal recovery during hotter months when the receiver temperature rises. Conversely, Melbourne and Sydney generate their highest heating outputs in January and December, Melbourne reaching 1,108,000 kWh and 1,109,360 kWh, respectively, corresponding to their winter season. Both cities exhibit a sharp decline in mid-year, dropping to as low as 35,984 kWh in July for Melbourne. This hemispheric inversion demonstrates the system's capacity to recover and redistribute thermal energy in response to changing ambient conditions. The results confirm the recuperator's effectiveness in improving seasonal heating performance and emphasize the value of climate-adaptive system configurations for year-round operation.

Fig. 14 presents the monthly cooling output generated by the system's evaporator, revealing distinct seasonal patterns driven by ambient temperature. Cooling production increases sharply during the warmer months, particularly in Isfahan and Ahvaz, which show the highest outputs between May and August. Isfahan peaks at 194,976 kWh in July, while Ahvaz reaches 157,176 kWh. In contrast, Melbourne and Sydney peak in January, producing 149,832 kWh and 165,888 kWh, respectively, and drop sharply mid-year. For example, Melbourne's cooling output falls to 2,197 kWh in June, compared to 160,272 kWh in Isfahan during the same month, illustrating the seasonal inversion between hemispheres. These results demonstrate the evaporator's responsiveness to elevated thermal loads and confirm the system's capacity to meet varying cooling demands across opposing seasonal cycles.

To further assess overall system adaptability, Table 11 summarizes the annual energy outputs for cooling, heating, and power across the four cities. Isfahan achieves the highest annual outputs, 1,446,790 kWh of cooling, 10,527,768 kWh of heating, and 1,629,562 kWh of power, due to its hot summers and cold winters, which impose high thermal loads. Ahvaz follows closely, also performing strongly across all three categories because of intense summer heat. In contrast, Sydney and Melbourne, located in the Southern Hemisphere, record lower annual outputs, particularly for cooling and heating, owing to their more temperate climates and milder seasonal extremes. These results represent gross plant-side outputs, including electricity produced by the solar Rankine cycle and thermal energy supplied to space heating, domestic hot water, and absorption cooling. Section 4.5 discusses surplus

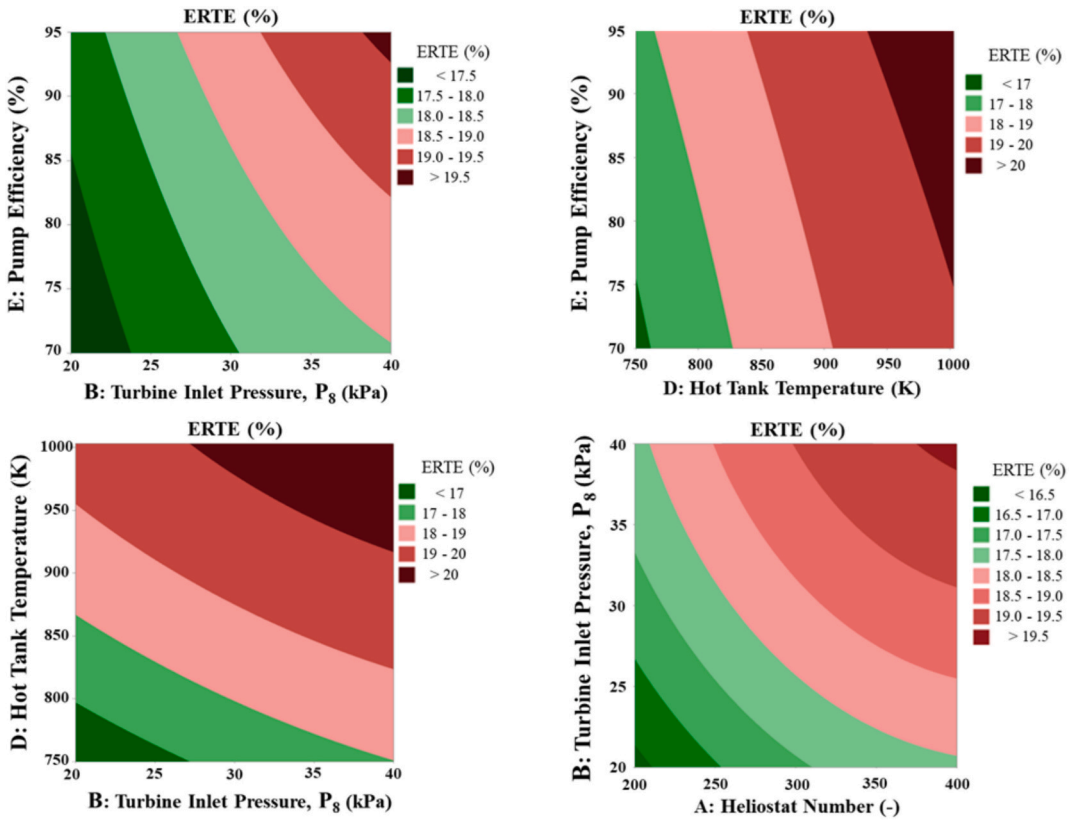

Fig. 8. Effects of input variables on exergy efficiency.

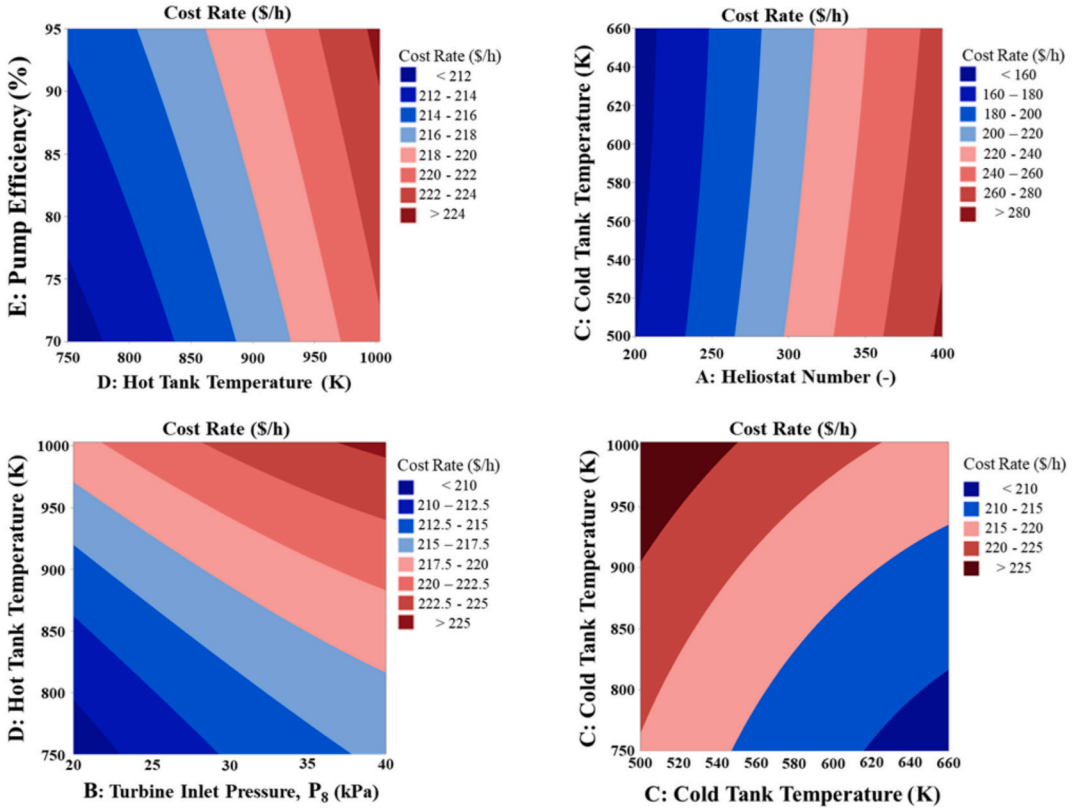

Fig. 9. Effects of Input variables on system cost rate.

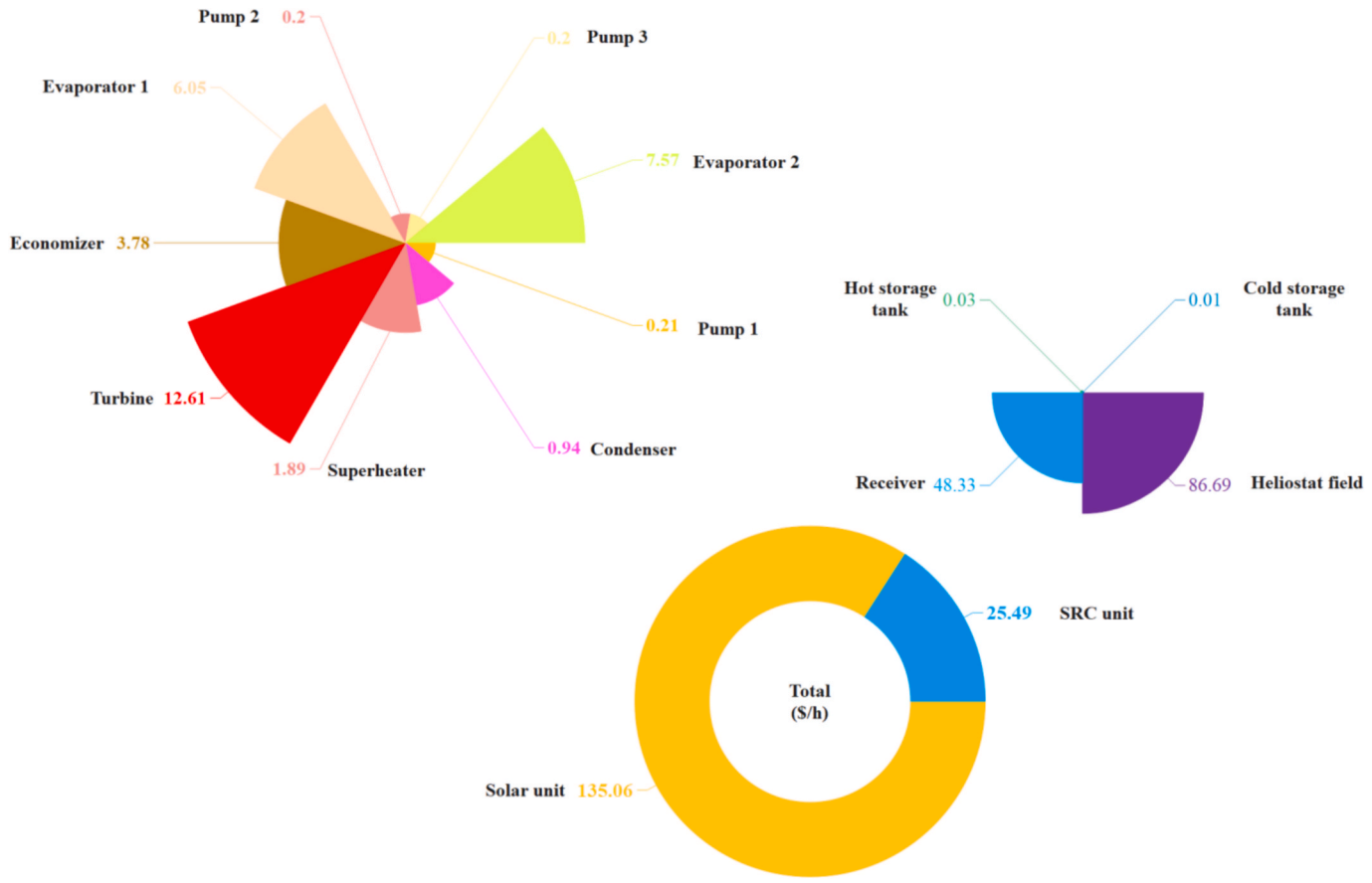

Fig. 10. Cost breakdown of system components.

generation relative to the 16-unit building's demand, which may be stored or exported. Overall, the results highlight the system's scalability and robustness across climates and confirm its suitability for deployment in regions with high year-round energy requirements.

Fig. 15 illustrates the monthly variation in CO_2 emissions, environmental cost, and land area required for carbon offsetting across Melbourne, Sydney, Ahvaz, and Isfahan, highlighting the system's environmental benefits. The results demonstrate clear seasonal and hemispheric patterns; Melbourne and Sydney record their highest CO_2 emissions and environmental costs in winter (June-August) due to elevated heating demand, whereas Ahvaz and Isfahan peak during summer (June–August), driven by high cooling requirements. Notably, Isfahan reaches the highest CO_2 emission intensity, exceeding 45 tons of CO_2 for July, while Melbourne's CO_2 output falls near zero in June and July. Similarly, environmental costs peak at over 1000 $ for Isfahan's July emissions, given the assumed CO_2 cost, reflecting the effect of extreme seasonal loads. The land area required to offset emissions follows a similar trend. Compared to a conventional power plant emitting 0.204 tons CO_2/MWh for 24 $/ton, the proposed system achieves substantial reductions in both emissions and costs during favorable months, supporting sustainable, low-carbon energy generation throughout the year. These outcomes align with recent findings in renewable system optimization studies [58,59].

Table 12 summarizes the system's annual environmental performance, revealing a direct correlation between net power output and associated CO_2 emissions, environmental cost, and offset land area. Isfahan, with the highest net power generation (1,629.6 MWh), also records the largest environmental footprint, 332.43 tons of CO_2, $7,978.33 in cost, and 1.61 for offsetting. Conversely, Melbourne, with the lowest power output (966.22 MWh), has the smallest environmental burden, 197.11 tons of CO_2, $4,730.63 in cost, and 0.95 ha. While higher generation increases emissions, the system remains notably cleaner than conventional alternatives, demonstrating potential for scalable, climate-responsive energy generation.

4.5. Energy storage potential

To further evaluate the efficiency and operational flexibility of the proposed multi-generation system, this section analyzes the monthly surplus of cooling, heating, and electricity across the studied cities. This assessment clarifies why the annual plant outputs presented in Table 11 exceed the building's annual demand: the system is intentionally optimized to ensure supply reliability year-round while generating controllable surpluses that can be directed toward energy storage or grid export. Understanding these surpluses is essential for identifying opportunities for energy redistribution, storage integration, and economic optimization.

Fig. 16 presents the monthly distribution of surplus electricity, heating, and cooling categorized as stored or excess energy. The electricity surplus was calculated by comparing turbine-generated power with the building's electricity consumption. The excess electricity can either be stored for later use or sold back to the grid, providing an additional revenue stream and enhancing the system's overall economic efficiency. The results show that Isfahan and Ahvaz achieved the highest surplus electricity during May to August, with Isfahan peaking at 208,462 kWh in July, reflecting high solar availability. In contrast, Melbourne and Sydney exhibit surplus electricity mainly in December and January, consistent with Southern Hemisphere solar peaks.

For surplus heating, Isfahan demonstrates the largest values, exceeding 1.4 million kWh in July, followed closely by Ahvaz, reflecting efficient thermal energy recovery in high-temperature conditions. Conversely, Melbourne and Sydney generate most of their heating

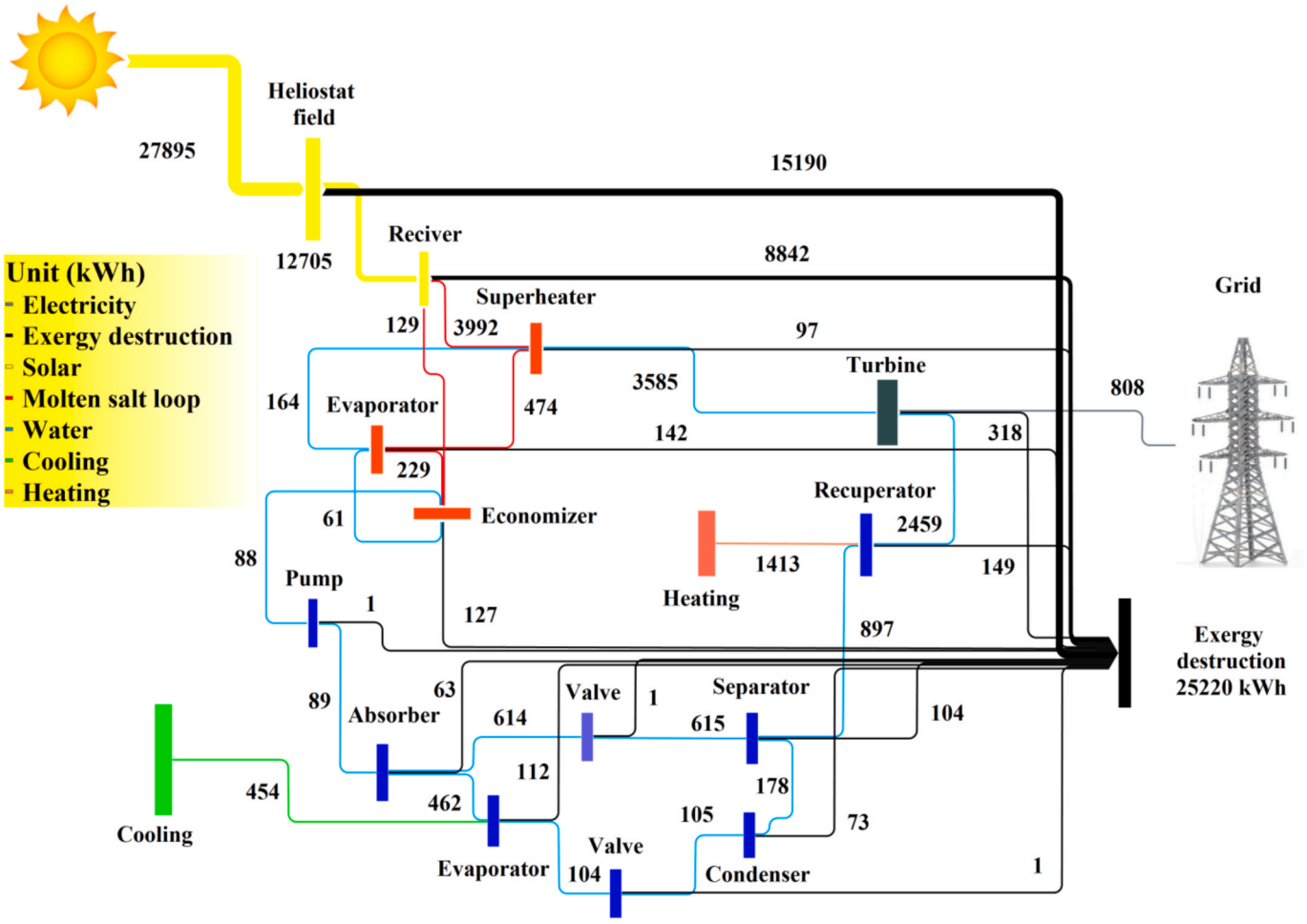

Fig. 11. Exergy flow and losses of the system under optimal conditions.

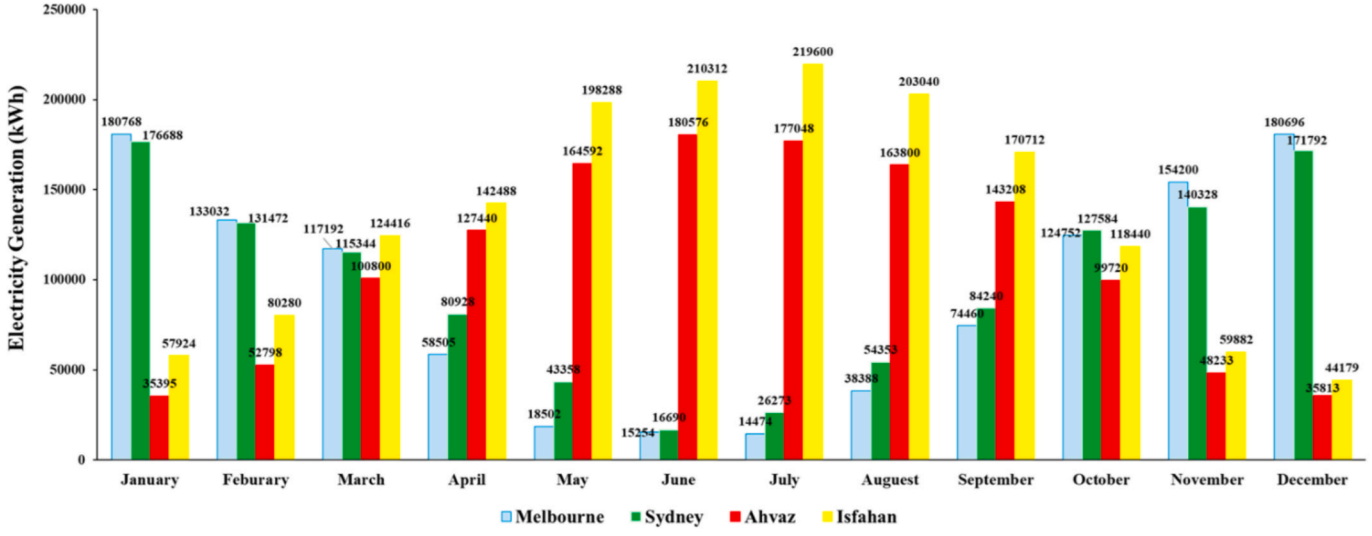

Fig. 12. Monthly net power output across the study cities.

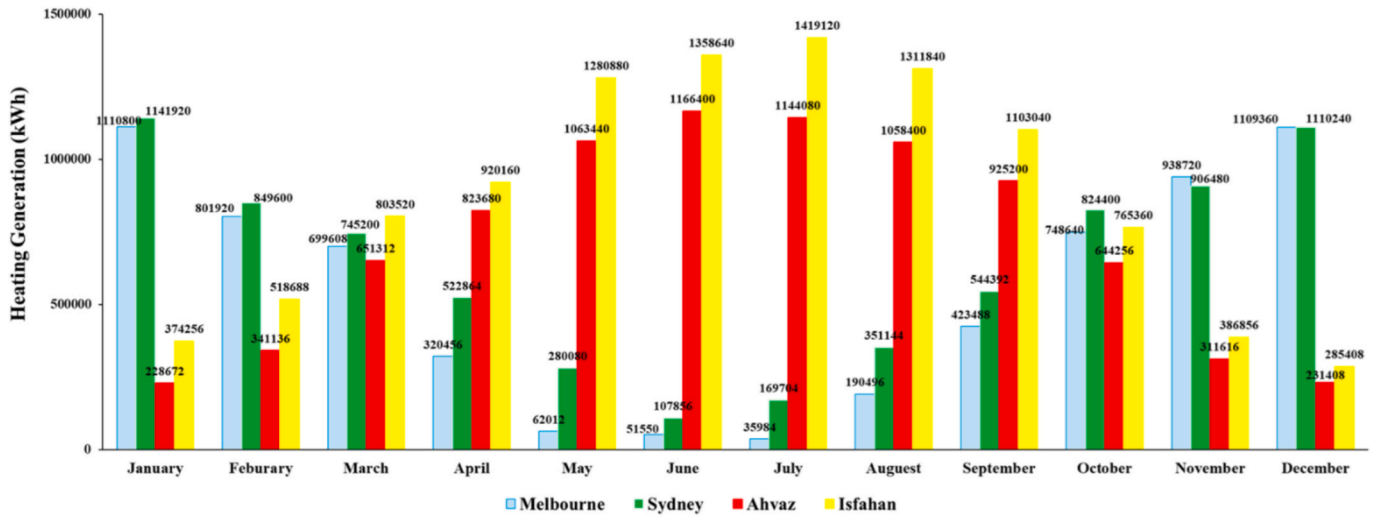

Fig. 13. Monthly heating output from the recuperator in selected cities.

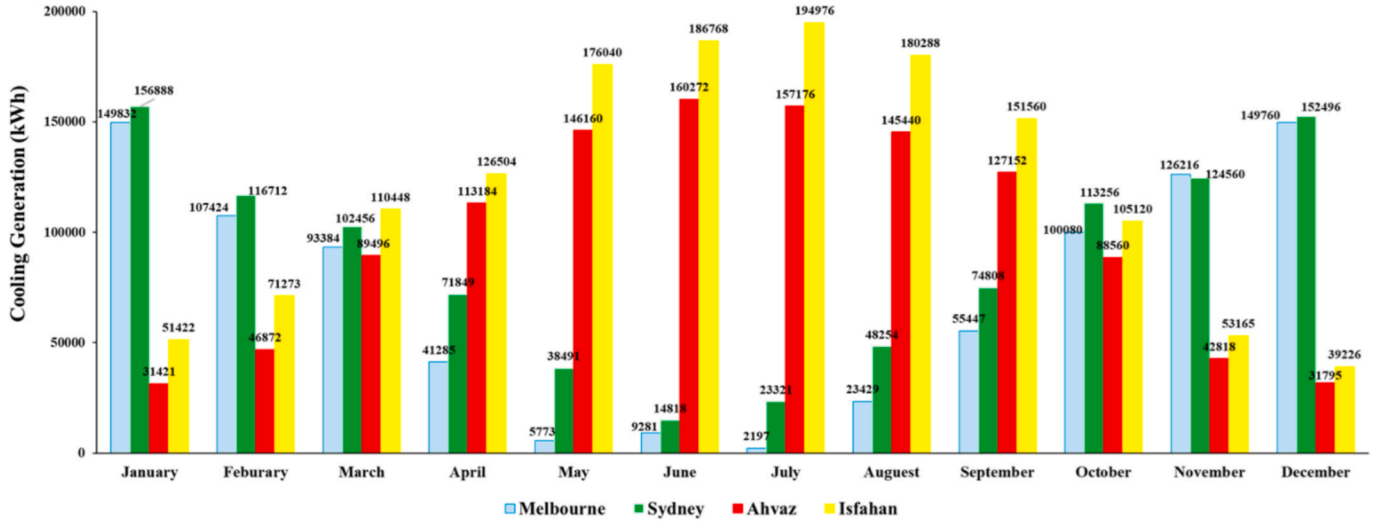

Fig. 14. Monthly cooling output from the evaporator reflecting seasonal cooling demand.

surplus during winter (June–August), with Melbourne reaching 1.1 million kWh in July before declining in mid-year. Cooling surpluses display an inverse seasonal pattern, with Isfahan and Ahvaz peaking during the Northern Hemisphere summer, Isfahan reaching 154,203 kWh in May, while Melbourne's cooling surplus drops to just over 2,000 kWh in winter. These findings confirm the system's seasonal adaptability and demonstrate its capacity to balance energy supply and demand through thermal storage or export mechanisms, contributing to a resilient and economically sustainable clean-energy strategy across diverse climate zones.

Table 11
Annual energy performance results of the system in studied cities.

Energy production	Unit	Selected city			
		Sydney	Ahvaz	Isfahan	Melbourne
Cooling	kWh	1,037,909	1,180,346	1,446,790	864,107
Heating	kWh	7,553,880	8,589,600	10,527,768	6,493,034
Power	kWh	1,169,050	1,329,422	1,629,562	1,110,223

4.6. Scalability and system flexibility

The scalability of the proposed multi-generation system was critically assessed by analyzing its modular components, including the heliostat array, SRC, and thermal storage units. By adjusting the number of heliostats, turbine inlet pressures, and thermal storage capacities, the system can be precisely scaled up or down to meet diverse residential or district-scale energy demands. For example, expanding the heliostat field in Isfahan or Ahvaz could substantially increase electricity generation, supporting community-scale cooling and heating needs without major modifications to the core system configuration. The integration of advanced predictive controls and machine learning-driven optimization could dynamically manage system capacity and storage operations, enhancing adaptability and ensuring efficient performance under variable load conditions. In practice, the plant can be downscaled to serve a 16-unit complex or upscaled for district-level applications. The gross outputs shown in Table 11 represent a robustness-oriented configuration, designed to produce seasonal surpluses for storage or export.

System flexibility is strengthened by its capacity to manage and redistribute energy surpluses, enabling strategic energy storage and smart grid integration. A particularly innovative feature is the system's

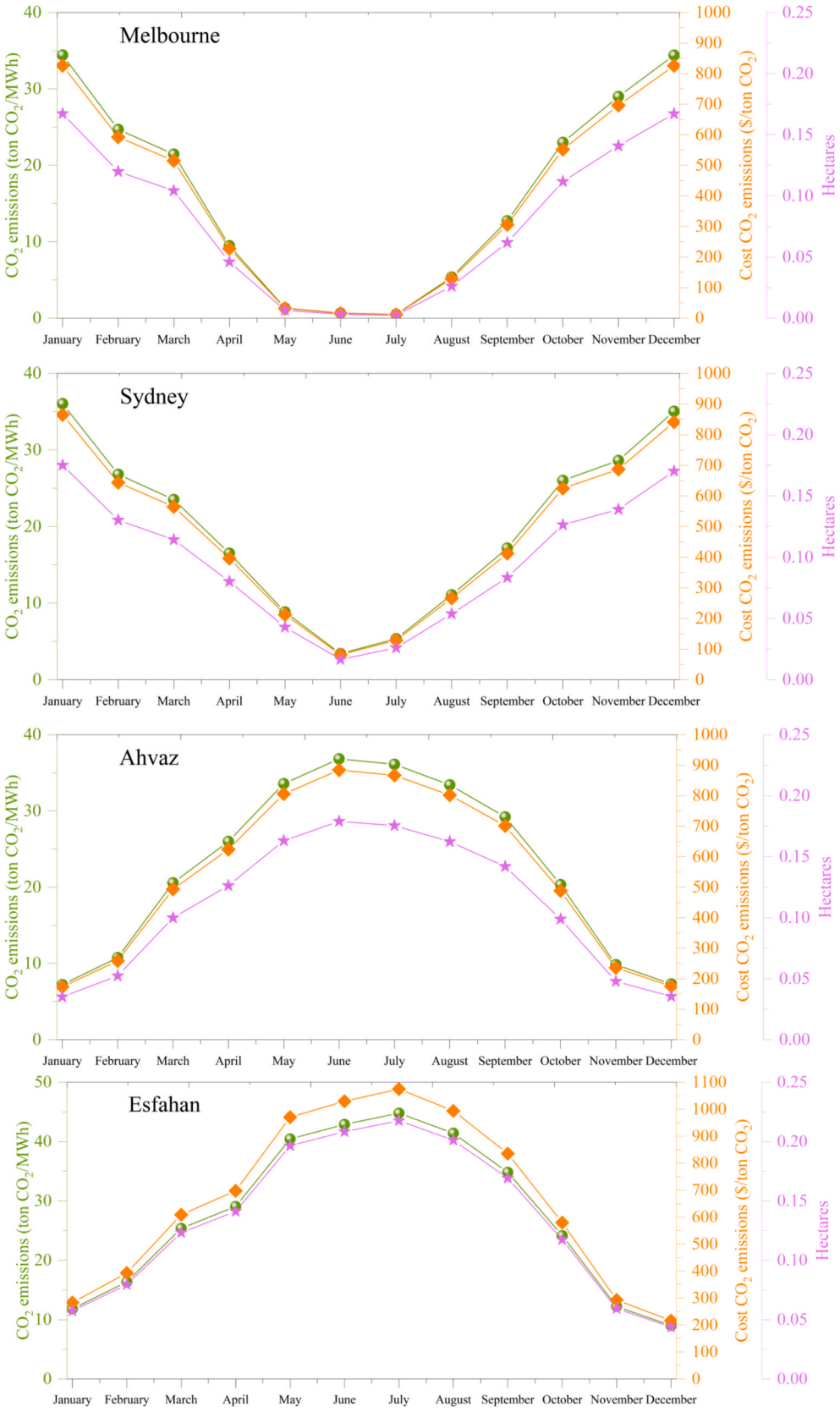

Fig. 15. Monthly CO_2 emissions, environmental costs, and offset potential in studied cities.

Table 12
Annual environmental performance related to power production in the studied cities.

City	Output net power (MWh)	CO_2 emissions ($tonCO_2$/MWh)	CO_2 cost ($/$tonCO_2$)	Hectares
Sydney	1169.050	238.486	5723.667	1.150
Ahvaz	1329.422	271.202	6508.852	1.310
Isfahan	1629.562	332.431	7978.334	1.610
Melbourne	966.223	197.107	4730.630	0.950

potential integration with Electric Vehicle (EV) charging infrastructure, where surplus solar electricity generated during peak hours can directly power EV fleets, reducing grid dependency and supporting urban decarbonization goals. Similarly, thermal energy surpluses may be redirected to absorption chillers or district heating networks, contributing to multi-functional urban energy hubs. By leveraging IoT-enabled energy management platforms, real-time monitoring and control of these dynamic interactions would allow rapid responses to fluctuating demands, energy tariffs, and climatic conditions, establishing the system

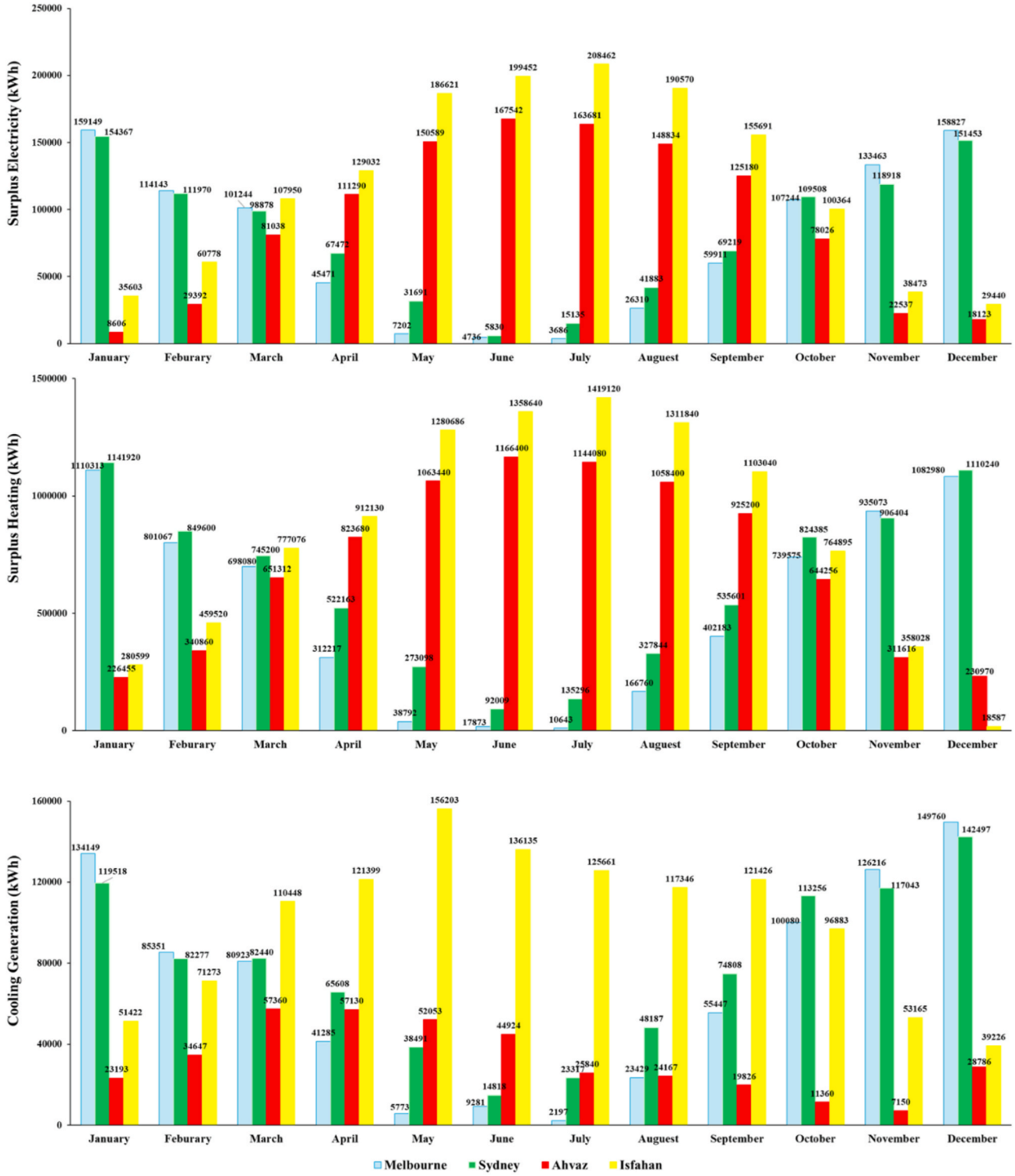

Fig. 16. Monthly surplus electricity, heating, and cooling in the studied cities.

as a flexible, scalable, and future-ready solution for sustainable urban energy systems.

The results demonstrate robust performance across diverse climates and hemispheric conditions, confirming the system's viability and scalability. However, additional performance gains may be achieved through advanced thermal storage integration, improved receiver designs, or hybrid renewable energy coupling (e.g., geothermal or wind systems). These improvements would enhance overall efficiency and cost-effectiveness, addressing remaining constraints in solar concentration and thermal transfer efficiency, particularly at the heliostat and receiver stages.

Beyond performance enhancement, the study's findings provide a practical basis for system design and policy implementation in sustainable residential energy development. Validated parameters such as turbine inlet pressure, heliostat number, and storage temperature serve as benchmarks for modular prototype development adaptable to different climates. Furthermore, the integrated BEopt–EES–RSM optimization framework offers a reproducible decision-support tool for engineers, planners, and policymakers to evaluate renewable configurations under site-specific conditions. The demonstrated hemispheric robustness establishes a transferable blueprint for implementing similar multi-generation systems in regions with reversed seasonal patterns, contributing directly to net-zero housing initiatives and broader decarbonization objectives.

5. Limitations and future directions

This study acknowledges methodological and practical limitations that define clear opportunities for future research and system refinement. Firstly, the performance simulations are based on idealized weather datasets and assume uniform user-demand profiles throughout the year. These assumptions may not fully capture real-world consumption behaviors, which are influenced by occupant habits, socio-economic factors, and climate variability. The economic evaluation also assumes static market conditions and fixed electricity prices, potentially overlooking fluctuations in energy tariffs, government incentives, maintenance costs, and system degradation over time. In terms of environmental assessment, the analysis focuses solely on CO_2 emissions, without considering other pollutants or full lifecycle impacts, including those associated with component manufacturing, installation, and end-of-life disposal.

To address these limitations and enhance the applicability of the proposed framework, several future research directions are recommended. Experimental validation under real-world urban occupancy and climate conditions would provide critical insights into practical operation, user behavior, and system reliability. Incorporating dynamic pricing models, demand-response mechanisms, and predictive analytics could improve economic optimization under fluctuating market conditions. Expanding the environmental assessment to include comprehensive lifecycle analysis and broader emission metrics would yield a more holistic understanding of the system's sustainability profile. Furthermore, integrating complementary renewable energy sources, such as photovoltaic, geothermal, or wind systems, and hybrid energy storage technologies (e.g., battery-electric, thermal, or hydrogen storage) could significantly enhance system flexibility, resilience, and long-term sustainability. Targeted technological advancements in heliostat field efficiency, adaptive receiver designs, and high-capacity thermal storage systems are also expected to reduce exergy losses and further improve overall system performance. These developments would pave the way toward next-generation zero-energy urban systems capable of operating reliably under diverse climatic and economic conditions.

6. Conclusion

This study designed and optimized a solar-driven multi-generation energy system capable of reliably meeting residential electricity, heating, and cooling demands across contrasting hemispheric climates. By integrating BEopt building simulations, thermodynamic modeling via Engineering Equation Solver (EES), and multi-objective optimization via Response Surface Methodology (RSM), the research evaluated system performance across four climatically diverse cities: Sydney, Melbourne, Ahvaz, and Isfahan. Under optimal conditions, the system achieved a maximum exergy efficiency of 19.42 %, producing 1,629.6 MWh of electricity, 10,527.8 MWh of heating, and 1,446.8 MWh of cooling in Isfahan. It also reduced annual CO_2 emissions by 332.43 tons and achieved a minimum operational cost rate of $169.93/hour, consistently generating surplus energy suitable for storage or grid integration. These outcomes confirm the effectiveness of the proposed multi-objective optimization approach and demonstrate the system's potential as a globally adaptable, cost-effective, and environmentally sustainable residential energy solution.

The key contribution of this research lies in its comparative assessment of the system's performance under reversed seasonal conditions and diverse climatic contexts, providing new insights into hemispheric variability and practical design strategies. The comprehensive methodological framework developed here advances current knowledge by demonstrating how optimal design parameters can effectively balance energy outputs and costs, establishing a foundation for widespread implementation of multi-generation systems across different regions. Through predictive modeling and advanced optimization, this study achieves improvement over existing approaches, particularly in exergy efficiency, economic viability, and environmental performance. Although the achieved efficiency gains are incremental rather than transformative, the systematic and adaptable methodology enhances real-world applicability and supports future system deployment.

Looking ahead, this work outlines a clear pathway for continued research and practical development to enhance sustainability and scalability:

- Integration of hybrid solar-geothermal configurations to improve year-round thermal performance.
- Development and deployment of advanced energy storage solutions to effectively manage surplus production.
- Implementation of real-time demand-response mechanisms for improved operational efficiency.
- Comprehensive lifecycle and techno-economic analyses to evaluate long-term system viability.

Ultimately, this research provides a replicable and adaptable energy model that can contribute to the global transition toward resilient, efficient, and sustainable residential energy systems, addressing both climatic variability and growing energy demands.

Declaration of generative AI and AI-assisted technologies in the writing process

During the preparation of this work, the authors used an OpenAI tool to enhance language and readability. After using the tool, the authors reviewed and edited the content as needed. They take full responsibility for the final content of the publication. The authors highlight that AI's role was to assist in refining the text and language, and not to replace any critical tasks of the authors.

Declaration of competing interest

The authors declare that they have no known competing financial interests or personal relationships that could have appeared to influence the work reported in this paper.

Appendix A. . System modeling parameters and performance evaluation equations

The appendix provides key technical details supporting the study's analysis. Table A1 outlines basic principles like mass and energy conservation and exergy balance, essential for modeling system performance. Table A2 lists input data, including environmental conditions and system parameters. Table A3 details the energy balance for system components such as the turbine, pump, and evaporator. Eqs. (A.1) and (A.2) calculate system output power and exergy efficiency. Lastly, Table A4 provides cost relations and auxiliary equations for evaluating the system's economic performance. This section ensures clarity and transparency in the methodology used.

Table A1
Basic relationships applied in the system analysis.

Fundamental Relationships	Relationship
Mass Conservation	$\sum \dot{m}_i - \sum \dot{m}_e = \frac{dm_{cv}}{dt}$
Energy Conservation	$\dot{Q} - \dot{W} + \sum_i \dot{m}_i \left(h_i + \frac{v_i^2}{2} + gZ_i \right) - \sum_e \dot{m}_e \left(h_e + \frac{v_e^2}{2} + gZ_e \right) = \frac{dE_{cv}}{dt}$
Exergy Balance	$\dot{E}x_Q + \sum_i \dot{m}_i (ex_i) = \sum_e \dot{m}_e (ex_e) + \dot{E}x_w + \dot{E}x_D$
Physical Exergy	$\dot{E}x_{ph} = \sum_i \dot{m}_i ((h_i - h_0) - T_0 (s_i - s_0))$
Cost Rate	$\dot{Z} = \frac{Z \times CRF \times \varphi}{T}$
Capital Recovery Parameter	$CRF = \frac{k(1+k)^n}{(1+k)^n - 1}$

Table A2
Input data used for system simulation.

Data	Unit	Value
T_0	K	298.15
P_0	kPa	101.3
N_{hel}	–	250
DNI	W/m^2	850
T_{sun}	K	6273.15
v	m/s	5
$T_{tank.hot}$	K	773.15
$T_{Cank.cold}$	K	573.15
η_{pump}	%	80
η_{Tur}	%	80
ε	%	90
σ	W/m^2.K^4	5.67 × 10^{-8}
P_8	kPa	32
T_{17}	K	313.15

Table A3
Energy balance relationships of the system components.

System components	Relationship
Turbine	$\dot{W}_{tur} = \dot{m}_8 \times (h_8 - h_9)$
Pump	$\dot{W}_{pump} = \dot{m}_{17} \times (h_{17} - h_7)$
Evaporator	$Q_{evap} = \dot{m}_{14} \times (h_{14} - h_{13})$
Condenser	$\dot{Q}_{Cond} = \dot{m}_{11} \times (h_{12} - h_{11})$
Superheater	$\dot{Q}_{SH} = \dot{m}_5 \times (h_5 - h_6)$
Economizer	$\dot{Q}_{eco} = \dot{m}_7 \times (h_7 - h_8)$
Absorber	$\dot{Q}_{abs} = \dot{m}_{14 \to 16} \times (h_{17} - h_{14} + h_{16})$

The output power is calculated by Eq. (A1):

$$\dot{W}_{net} = \dot{W}_{Tur} - \dot{W}_{pump} \tag{A1}$$

Eq. (A2) is used to calculate the system ERTE:

$$ERTE = \frac{(\dot{W}_{net} + \dot{E}x_{cooling} + \dot{E}x_{heating})}{\dot{E}_{sun}} \times T_{discharge} \times 100 \tag{A.2}$$

In Table A4, the cost relationships for each system component, along with the necessary auxiliary equations, are provided. These relations are essential for evaluating the economic aspects of the system, offering a clear framework for calculating both component costs and overall system

expenses. The inclusion of auxiliary equations further supports detailed financial analysis, ensuring comprehensive cost evaluation:

Table A4
Cost and auxiliary relations for system components.

System Components	Relationship
Receiver	$\dot{Z}_{rec} = A_{rec} \times (79T - 42000)\dot{Z}$
Heliostat	$\dot{Z}_{hel} = 150 \times A_{hel} \times N_{hel} \times \dot{Z}$
Turbine	$\dot{Z}_{tur} = [4750\left(\dot{W}_{tur}\right)^{0.75} + 60\left(\dot{W}_{tur}\right)^{0.95}]\dot{Z}$
Pump	$\dot{Z}_{pump} = 3500 \times \left(\dot{W}_{pump}\right)^{0.41} \times \dot{Z}$
Condenser	$\dot{Z}_{cond} = 150 \times (A_{cond})^{0.8} \times \dot{Z}$
Evaporator	$\dot{Z}_{evap} = 276 \times (A_{evap})^{0.88} \times \dot{Z}$
Cold Storage Source	$\dot{Z}_{tank,cold} = 5941.7 \times (V_{tank,cold})^{-0.289} \times \dot{Z}$
Hot Storage Source	$\dot{Z}_{tank,hot} = 5941.7 \times (V_{tank,hot})^{-0.272} \times \dot{Z}$
Superheater	$\dot{Z}_{SH} = 276 \times (A_{SH})^{0.88} \times \dot{Z}$
Economizer	$\dot{Z}_{eco} = 276 \times (A_{eco})^{0.88} \times \dot{Z}$
Recuperator	$\dot{Z}_{rec} = 12000 \times \left(\frac{A_{Rec}}{100}\right)^{0.88} \times \dot{Z}$

Appendix B. . Optimization dataset generated via response surface methodology

The optimization process employed RSM using Minitab to explore the effects of six decision variables on system performance. These include heliostat number, turbine inlet pressure (P8), cold and hot tank temperatures, pump efficiency, and turbine efficiency. A total of 90 simulation runs were generated using EES and assessed for two key objective functions: ERTE and cost rate. This extensive dataset forms the backbone of the multi-objective optimization, enabling accurate regression modeling and desirability analysis.

Table B1
Complete design matrix of 90 RSM optimization runs.

Run	Heliostat number (−)	P8 (kPa)	Cold tank temperature (K)	Hot tank temperature (K)	Pump efficiency (%)	Turbine efficiency (%)	ERTE (%)	Cost rate ($/h)
1	300	30	575	825	0.825	0.825	18.37	215.1
2	400	40	500	900	0.95	0.7	21.25	291.6
3	400	20	500	900	0.7	0.7	18.94	279.2
4	200	20	500	900	0.7	0.95	16.82	159.6
5	300	30	575	825	0.825	0.825	18.37	215.1
6	300	22	575	825	0.825	0.825	17.64	212
7	200	40	650	900	0.95	0.7	18.87	159.2
8	200	20	500	750	0.95	0.95	15.78	153.7
9	300	30	575	825	0.825	0.825	18.37	215.1
10	300	30	575	825	0.825	0.825	18.37	215.1
11	300	30	575	825	0.825	0.93	18.38	215.1
12	300	24	575	825	0.825	0.825	17.85	212.9
13	200	20	500	900	0.7	0.95	16.82	159.6
14	200	40	650	900	0.7	0.95	17.93	156.5
15	200	20	500	750	0.7	0.7	15.15	152
16	300	30	575	825	0.825	0.825	18.37	215.1
17	200	40	650	900	0.7	0.95	17.93	156.5
18	200	40	650	900	0.7	0.95	17.93	156.5
19	300	30	660	825	0.825	0.825	18.37	210.3
20	200	20	650	900	0.95	0.95	17.29	153.9
21	200	40	650	750	0.95	0.95	17.8	151.4
22	200	20	500	900	0.7	0.95	16.82	159.6
23	200	20	650	900	0.7	0.7	16.81	152.3
24	300	30	575	825	0.8	0.825	18.28	214.8
25	250	30	575	825	0.825	0.825	17.95	185.1
26	300	30	575	825	0.825	0.825	18.37	215.1
27	200	20	650	900	0.95	0.95	17.29	153.9
28	300	30	540	825	0.825	0.825	18.37	218.1
29	300	30	575	825	0.825	0.825	18.37	215.1
30	300	30	575	1003	0.825	0.825	20.18	223.1
31	400	20	650	900	0.7	0.95	18.95	264.3
32	200	40	650	750	0.7	0.7	16.51	148.7
33	400	40	650	900	0.95	0.95	21.28	276.5
34	300	30	575	825	0.825	0.825	18.37	215.1
35	300	30	575	825	0.825	0.825	18.37	215.1
36	300	30	575	810	0.825	0.825	18.15	214.5
37	400	20	500	900	0.95	0.95	19.47	282.1
38	300	30	575	825	0.92	0.825	18.73	216.3
39	400	20	650	900	0.7	0.95	18.95	264.3

(*continued on next page*)

Table B1 (*continued*)

Run	Heliostat number (−)	P8 (kPa)	Cold tank temperature (K)	Hot tank temperature (K)	Pump efficiency (%)	Turbine efficiency (%)	ERTE (%)	Cost rate ($/h)
40	200	20	500	750	0.95	0.95	15.78	153.7
41	300	30	575	890	0.825	0.825	19.24	217.9
42	300	30	575	825	0.9277	0.825	18.75	216.4
43	310	30	575	825	0.825	0.825	18.44	221.1
44	200	40	500	900	0.7	0.7	17.9	163.9
45	200	40	650	900	0.95	0.7	18.87	159.2
46	400	40	650	750	0.7	0.95	17.61	269
47	200	20	650	750	0.7	0.95	15.17	144.2
48	400	20	500	900	0.7	0.7	18.94	279.2
49	400	20	500	900	0.95	0.95	19.47	282.1
50	300	25	575	825	0.825	0.825	17.95	213.3
51	340	30	575	825	0.825	0.825	18.62	239
52	400	20	500	900	0.95	0.95	19.47	282.1
53	300	22	575	825	0.825	0.825	17.64	212
54	300	30	575	825	0.825	0.825	18.37	215.1
55	400	20	650	900	0.95	0.7	19.46	267.4
56	400	40	500	750	0.7	0.7	17.58	284
57	300	30	575	825	0.825	0.9528	18.38	215.1
58	300	30	575	825	0.825	0.825	18.37	215.1
59	300	30	575	825	0.825	0.825	18.37	215.1
60	300	30	575	770	0.825	0.825	17.51	213
61	200	40	500	900	0.7	0.7	17.9	163.9
62	400	40	650	750	0.95	0.7	18.92	273.9
63	200	20	650	750	0.95	0.7	15.76	146
64	200	40	500	750	0.7	0.95	16.54	156.4
65	200	40	500	900	0.7	0.7	17.9	163.9
66	400	40	650	750	0.7	0.95	17.61	269
67	400	40	500	750	0.95	0.95	18.96	288.5
68	300	30	575	825	0.825	0.825	18.37	215.1
69	400	40	650	900	0.7	0.7	20.16	271.9
70	300	30	575	860	0.825	0.825	18.86	216.6
71	200	20	500	900	0.95	0.7	17.28	161.3
72	400	40	500	900	0.7	0.95	20.19	286.7
73	300	30	575	825	0.825	0.825	18.37	215.1
74	200	20	650	750	0.7	0.95	15.17	144.2
75	400	40	500	900	0.7	0.95	20.19	286.7
76	200	20	650	750	0.95	0.7	15.76	146
77	200	40	650	750	0.7	0.7	16.51	148.7
78	400	20	650	900	0.7	0.95	18.95	264.3
79	200	20	650	750	0.7	0.95	15.17	144.2
80	400	20	500	750	0.95	0.7	16.78	279.3
81	300	30	575	825	0.825	0.825	18.37	215.1
82	400	20	500	750	0.95	0.7	16.78	279.3
83	400	20	500	750	0.7	0.95	16.16	276.1
84	300	30	575	825	0.825	0.825	18.37	215.1
85	400	20	650	900	0.95	0.7	19.46	267.4
86	200	40	650	750	0.95	0.95	17.8	151.4
87	400	40	650	900	0.95	0.95	21.28	276.5
88	400	20	650	750	0.95	0.95	16.8	264.5
89	400	20	500	750	0.95	0.7	16.78	279.3
90	200	40	500	900	0.95	0.95	18.89	166.5

Data availability

Data will be made available on request.

References

[1] United Nations Environment Programme (UNEP) and Global Alliance for Buildings and Construction, Not just another brick in the wall: The solutions exist - scaling them will build on progress and cut emissions fast. Global Status Report for Buildings and Construction 2024/2025. (2025).

[2] Cabeza, L.F., Bai, Q., Bertoldi, P., Kihila, J. M., Lucena, A. F. P., Mata, É., Mirasgedis, S., Novikova, A., Saheb, Y., Climate Change 2022: Mitigation of Climate Change. Contribution of Working Group III to the Sixth Assessment Report of the Intergovernmental Panel on Climate Change. 2022: Cambridge, UK and New York, NY, USA. p. Chapter 9, pp. 953–1018.

[3] International Energy Agency (IEA), Energy Efficiency 2024 – Analysis. 2024: Paris.

[4] United Nations (UN). *Sustainable Development Goals*. 2015 [cited 2025 October 20, 2025]; Available from: http://sdgs.un.org/goals.

[5] International Energy Agency (IEA), Global Energy Review 2025 – Analysis. 2025.

[6] A. Lakhouit, et al., Assessing the environmental impact of PV emissions and sustainability challenges, Sustainability (2071–1050) 17 (7) (2025).

[7] J. Wu, et al., Residential solar photovoltaic adoption: an in-depth review on potential, main barriers and related incentives, Energ. Buildings (2025) 115766.

[8] A.A. Rathod, et al., A holistic approach to multi-generation energy systems performance: optimization with energy and exergy analysis, Electr. Eng. (2025) 1–21.

[9] G. Wang, Z. Zhang, J. Lin, Multi-energy complementary power systems based on solar energy: a review, Renew. Sustain. Energy Rev. 199 (2024) 114464.

[10] A. Allouhi, M.B. Amine, C. Reisch, Multi-objective optimization of solar energy systems for electricity and hot water generation in collective residential buildings considering the power-to-heat concept, Appl. Therm. Eng. 230 (2023) 120658.

[11] Y. Liu, et al., Modeling and exergy-economy analysis of residential building energy supply systems combining torrefied biomass gasification and solar energy, Therm. Sci. Eng. Prog. 50 (2024) 102584.

[12] Z. Mao, et al., Exergo-economic analysis and multi-objective optimization of a novel solar-driven multigeneration system for efficient energy utilization, Appl. Therm. Eng. (2025) 127512.

[13] B. Wang, et al., A review of the photothermal-photovoltaic energy supply system for building in solar energy enrichment zones, Renew. Sustain. Energy Rev. 191 (2024) 114100.

[14] B. Senyonyi, H. Mahmoud, H. Hassan, Systematic review of solar techniques in zero energy buildings, Clean Techn. Environ. Policy 27 (2) (2025) 727–772.

[15] E. Assareh, et al., Application of a multi-objective approach integrating solar-wind co-generation with response surface method to optimize zero-energy buildings, Appl. Therm. Eng. 265 (2025) 125637.
[16] N. Tong, Thermoeconomic and environmental assessment of a solar-based trigeneration unit, Appl. Therm. Eng. (2025) 127531.
[17] X. Guo, Y. Han, L. Ma, J. Zhang, Optimization and year-round trigeneration performance analysis of the photovoltaic thermal heat pump system: a case of engineering application, Energy 333 (2025).
[18] D.B.M. Delgado, I. Costa e Silva Neto, M. Carvalho, Strategies for multigeneration in residential energy systems: an optimization approach, Sustainability 17 (3) (2025) 1016.
[19] B. Eyyamoglu, K. Bahlouli, Performance and economic analysis of a nanofluid-based solar-driven trigeneration system for a residential building in Cyprus, Appl. Therm. Eng. (2025) 127001.
[20] Y. Xie, et al., Application benefit evaluation and two-stage co-optimization of solar hybrid CCHP systems with energy storage based on climate regions and building types, Appl. Therm. Eng. (2025) 128429.
[21] M. De Rosa, M. Aliehyaei, Techno-economic and environmental assessment of a solar-powered multi-generation system for a sustainable energy, hydrogen and fresh-water production, Therm. Sci. Eng. Prog. (2025) 103856.
[22] M. Deymi-Dashtebayaz, et al., Comparison of two hybrid renewable energy systems for a residential building based on sustainability assessment and emergy analysis, J. Clean. Prod. 379 (2022) 134592.
[23] P. Hajialigol, A. Fathi, Y. Saboohi, Modeling and optimization of an integrated multi-generation solar system with variable heat to power ratio for supplying residential and industrial demands, Renew. Energy 174 (2021) 786–798.
[24] M. Jafarian, et al., Energy, economic, and environmental analysis of combined cooling, heat, power and water (CCHPW) system incorporated with photovoltaic/thermal collectors and reverse osmosis systems, J. Build. Eng. 75 (2023) 107059.
[25] E. Assareh, N. Agarwal, M. Lee, Zero energy building optimization for a residential complex with a new optimized cogeneration system for electricity, cooling, heating and freshwater production, Appl. Therm. Eng. 244 (2024) 122527.
[26] G. Mancò, et al., A review on multi energy systems modelling and optimization, Appl. Therm. Eng. (2023) 121871.
[27] S. Mobayen, et al., Dynamic analysis and multi-objective optimization of an integrated solar energy system for Zero-Energy residential complexes, Energ. Conver. Manage. 341 (2025) 119924.
[28] M. Thirunavukkarasu, Y. Sawle, H. Lala, A comprehensive review on optimization of hybrid renewable energy systems using various optimization techniques, Renew. Sustain. Energy Rev. 176 (2023) 113192.
[29] E.K. Quaye, et al., Advancing sustainable combustion: a comprehensive review of response surface methodology driven optimization and applications in alternative fuel combustion systems, Int. J. Hydrogen Energy 170 (2025) 151190.
[30] A.S. Roshani, et al., Optimization of a hybrid renewable energy system for off-grid residential communities using numerical simulation, response surface methodology, and life cycle assessment, Renew. Energy (2024) 121425.
[31] M. Reji, R. Kumar, Response surface methodology (RSM): an overview to analyze multivariate data, Indian J. Microbiol. Res. 9 (2022) 241–248.
[32] L. Liu, et al., Review of surrogate model assisted multi-objective design optimization of electrical machines: new opportunities and challenges, Renew. Sustain. Energy Rev. 215 (2025) 115609.
[33] M. Salahinezhad, et al., Trade-off analysis for optimal design of trigeneration energy systems integrated with solar and hydrogen subsystems: a novel optimization strategy, Renew. Energy 240 (2025) 122211.
[34] P. Jiang, Q. Zhou, X. Shao, Surrogate-model-based design and optimization, in: Surrogate Model-Based Engineering Design and Optimization, Springer, 2019, pp. 135–236.
[35] S. Yu, L. You, S. Zhou, A review of optimization modeling and solution methods in renewable energy systems, Front. Eng. Manag. 10 (4) (2023) 640–671.
[36] W. Chen, H. Ren, W. Zhou, Review of multi-objective optimization in long-term energy system models, Global Energy Interconnect. 6 (5) (2023) 645–660.
[37] M.S. Mohtasim, et al., Hybrid renewable multi-generation system optimization: attaining sustainable development goals, Renew. Sustain. Energy Rev. 212 (2025) 115415.
[38] C. Shan, et al., Multi-objective optimization of a novel combined cooling, heating and power solar thermal energy storage system: a comprehensive analysis of energy, exergy, exergoeconomic, and exergoenvironmental performance, Energy 316 (2025) 134464.
[39] A. Dezhdar, et al., Dynamic simulation and optimization of an innovative cogeneration system using TRNSYS, EES, and response surface methodology as a machine learning method, J. Taiwan Inst. Chem. Eng. 180 (2026) 106461.
[40] E. Assareh, et al., Techno-economic analysis of combined cooling, heating, and power (CCHP) system integrated with multiple renewable energy sources and energy storage units, Energ. Build. 278 (2023) 112618.
[41] J. Ran, et al., Coordinated optimization design of buildings and regional integrated energy systems based on load prediction in future climate conditions, Appl. Therm. Eng. 241 (2024) 122338.
[42] Q. Alfalouji, et al., Co-simulation for buildings and smart energy systems—a taxonomic review, Simul. Model. Pract. Theory 126 (2023) 102770.
[43] S. Di Fraia, et al., Solar-based systems, in: *Polygeneration Systems*, Elsevier, 2022, pp. 193–237.
[44] S. Ozlu, I. Dincer, Development and analysis of a solar and wind energy based multigeneration system, Sol. Energy 122 (2015) 1279–1295.
[45] S. Sami, M. Gholizadeh, M. Deymi-Dashtebayaz, An applicable multi-generation system for different climates from energy, exergy, exergoeconomic, economic, and environmental (5E) perspectives, Sustain. Cities Soc. 100 (2024) 105057.
[46] X. Ding, et al., Dynamic response characteristics and economic analyses of two solar-assisted multi-generation systems, Appl. Therm. Eng. 241 (2024) 122339.
[47] P. Gabrielli, et al., Optimal design of multi-energy systems with seasonal storage, Appl. Energy 219 (2018) 408–424.
[48] Meteotest, Meteonorm Version 8 – Climate Data Set. 2020, Meteotest.
[49] E.A. Rad, S. Mohammadi, E. Tayyeban, Simultaneous optimization of working fluid and boiler pressure in an organic Rankine cycle for different heat source temperatures, Energy 194 (2020) 116856.
[50] Minitab, L., Minitab 21 Statistical Software. (2022), Minitab, LLC: State College, PA, USA.
[51] A. Susaimanickam, P. Manickam, A.A. Joseph, A comprehensive review on RSM-coupled optimization techniques and its applications, Arch. Comput. Meth. Eng. 30 (8) (2023) 4831–4853.
[52] Peel, M.C., Finlayson, B. L., McMahon, T. A.,. Köppen–Geiger climate classification world map. 2016 [cited 2025 October 27]; Available from: https://koeppen-geiger.vu-wien.ac.at/.
[53] B. Mirletz, The 2024 Electricity Update. 2024, National Renewable Energy Laboratory (NREL), Golden CO, United States, 2024.
[54] International Renewable Energy Agency; International Energy Agency (IRENA), International Energy Agency (IEA), and Energy Technology Systems Analysis Programme (ETSAP), Technology Brief E10 – Concentrating Solar Power- Insights for Policy Makers. 2013, International Renewable Energy Agency (IRENA), in collaboration with International Energy Agency (IEA)- Energy Technology Systems Analysis Programme (ETSAP): Abu Dhabi.
[55] A. Tiktas, H. Gunerhan, A. Hepbasli, Single and multigeneration Rankine cycles with aspects of thermodynamical modeling, energy and exergy analyses and optimization: a key review along with novel system description figures, Energy Convers. Manage.: X 14 (2022) 100199.
[56] D.-Q. Li, et al., Response surface methods for slope reliability analysis: review and comparison, Eng. Geol. 203 (2016) 3–14.
[57] D.L. Allaix, V.I. Carbone, An improvement of the response surface method, Struct. Saf. 33 (2) (2011) 165–172.
[58] S.M. Alirahmi, et al., A comprehensive techno-economic analysis and multi-criteria optimization of a compressed air energy storage (CAES) hybridized with solar and desalination units, Energ. Conver. Manage. 236 (2021) 114053.
[59] T. Kroeger, et al., Reforestation as a novel abatement and compliance measure for ground-level ozone, Proc. Natl. Acad. Sci. 111 (40) (2014). E4204–E4213.